Ar–Ar and U–Pb ages of marble-hosted ruby deposits from central and southeast Asia

V. Garnier, H. Maluski, G. Giuliani, D. Ohnenstetter, and D. Schwarz

Abstract: To date the formation of ruby deposits and link it to the regional metamorphism associated with Tertiary Himalayan orogenesis, ^{40}Ar–^{39}Ar stepwise heating experiments were performed on single grains of phlogopite syngenetic with ruby, and zircon inclusions in ruby and spinel were dated with the U–Pb method by ion-probe. The Ar–Ar ages of phlogopites associated with ruby are Oligocene (24.7 ± 0.3 Ma) at Jegdalek in Afghanistan; Miocene at Mogok in Myanmar (18.7 ± 0.2 to 17.1 ± 0.2 Ma), at Hunza in Pakistan (10.8 ± 0.3 to 5.4 ± 0.3 Ma), and Chumar in Nepal (5.6 ± 0.4 Ma); and Pliocene (4.6 ± 0.1 Ma) at Ruyil in Nepal. In Vietnam, a zircon included in a ruby from the Quy Chau deposit yielded a ^{238}U–^{206}Pb age of 53.8 ± 4.6 Ma, whereas in the Red River shear zone, ruby formed at around 40–36 Ma during ductile deformation under peak metamorphic conditions. The ages obtained in this study are in agreement with those previously published for the ruby-bearing metamorphic belts and document extensional tectonics that were active from Afghanistan to Vietnam between the Oligocene and the Pliocene. Ruby-bearing marbles define a high-quality gem belt linked to the high-temperature metamorphism of the Himalayan fold belt that developed during the Tertiary collision of the Indian plate with Asia.

Résumé : Afin de dater la formation des gisements de rubis et de la relier au métamorphisme régional associé à l'orogenèse himalayenne, des datations ^{40}Ar–^{39}Ar par chauffage en paliers ont été réalisées sur des grains de phlogopite syngénétique du rubis, et des cristaux de zircon inclus dans des rubis et spindles ont été datés par la méthode U–Pb à la sonde ionique. Les âges des phlogopites associées au rubis sont oligocènes (24.7 ± 0.3 Ma) à Jegdalek en Afghanistan; miocènes à Mogok au Myanmar (18.7 ± 0.2 à 17.1 ± 0.2 Ma), à Hunza au Pakistan (10.8 ± 0.3 à 5.4 ± 0.3 Ma) et à Chumar au Népal (5.6 ± 0.4 Ma); et pliocènes (4.6 ± 0.1 Ma) à Ruyil au Népal. Un zircon inclus dans un rubis de Quy Chau au Viêt-nam donne un âge de 53.8 ± 4.6 Ma, tandis que dans la zone de cisaillement du Fleuve Rouge, le rubis s'est formé entre 40 et 36 Ma pendant la déformation ductile dans les conditions du pic de métamorphisme. Les âges obtenus dans cette étude sont en accord avec les principaux âges publiés pour les ceintures métamorphiques hôtes des marbres à rubis qui documentent la tectonique extensionnelle qui était active depuis l'Afghanistan jusqu'au Viêt-nam, de l'Oligocène au Pliocène. Les marbres à rubis forment une ceinture à gemmes de haute qualité reliée au métamorphisme de haute température de la chaîne himalayenne résultant de la collision tertiaire entre les plaques indienne et eurasienne.

[Traduit par la Rédaction]

Introduction

World-famous, economically viable marble-hosted ruby deposits are located within the Himalayan mountain belt that formed during the Tertiary collision of the Indian plate with Asia, and in the Indochina crustal block extruded along shear zones during this collision. Asian ruby deposits are widespread in metamorphic rocks, often intruded by granitic rocks, from Tadjikistan to Vietnam. The deposits of Jegdalek in Afghanistan are hosted by the sillimanite–garnet gneisses of western Nuristan (Debon et al. 1986). The deposits from the Hunza Valley in Pakistan are contained in the southern Karakoram metamorphic belt (Okrusch et al. 1976). Ruby deposits from Nangimali in Azad Kashmir are located in the southeastern termination of the Nanga Parbat spur (Pêcher et al. 2002). In Chumar and Ruyil in Nepal, the rubies are hosted in the kyanite–zoisite marbles located at the contact of the Main Central Thrust (MCT) (Smith et al. 1997). The famous ruby deposits from Mogok in Myanmar lay within the Mogok metamorphic belt (Bertrand et al. 2001). The Viet-

Received 22 February 2005. Accepted 19 January 2006. Published on the NRC Research Press Web site at http://cjes.nrc.ca on 11 May 2006.

Paper handled by Associate Editor W.J Davis.

V. Garnier, G. Giuliani,[1, 2] and D. Ohnenstetter. Centre de Recherches Pétrographiques et Géochimiques - Centre National de la Recherche Scientifique (CRPG-CNRS), UPR 2300, BP 20, 54501 Vandœuvre, France.
H. Maluski. Laboratoire de Géochronologie, Institut des Sciences de la Terre, de l'Eau et de l'Espace de Montpellier, Université de Montpellier 2, Place Eugène Bataillon, 34095 Montpellier CEDEX 05, France.
D. Schwarz. Gübelin Gemmological Laboratory, 102 Maihofstrasse, CH-6000 Lucerne 9, Switzerland.

[1]Corresponding author (e-mail: giuliani@crpg.cnrs-nancy.fr).
[2]UR154, LMTG UMR 5563, 14 Avenue Edouard Belin, 34000 Toulouse, France.

 doi:10.1139/E06-005

Fig. 1. Geological map of the Himalayan orogen illustrating the principal units and the ages of the main ruby and emerald deposits and plutonic intrusions in Afghanistan and Pakistan. Map modified after Debon et al. 1987 and Hildebrand et al. 2001; U–Pb ages from Schneider et al. (1999) and Fraser et al. (2001); ^{40}Ar–^{39}Ar ages from Dilles et al. (1994), Sabot et al. (2002) and this study; K–Ar and Rb–Sr ages from Debon et al. (1987).

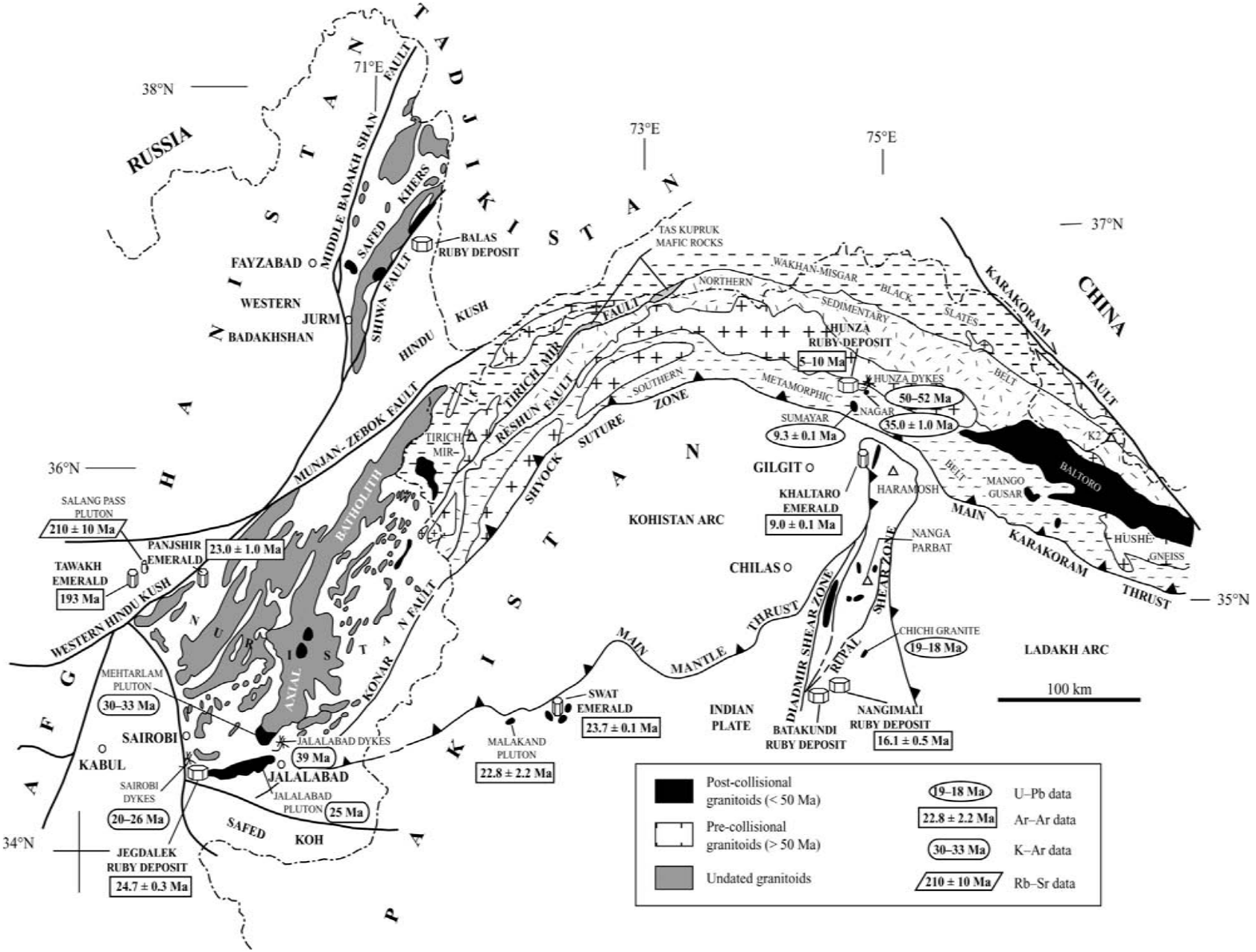

namese ruby deposits are hosted by metamorphic belts that are associated with large-scale shear zones, such as the Dai Nuy Con Voi metamorphic belt in the Red River shear zone that contains the deposits of Luc Yen and Yen Bai in the north and the Bu Khang dome, associated with the Quy Chau shear zone in central Vietnam.

The host rocks of the ruby deposits consist of a variety of strongly metamorphosed and deformed rocks including Al-rich garnet–biotite–sillimanite gneisses, schists, quartzites, amphibolites, and marbles. These rocks underwent high-temperature, amphibolitic to granulitic regional metamorphism (Okrusch et al. 1976; Bender 1983; Crawford and Searle 1993; Hauzenberger et al. 2001; Leloup et al. 2001). The age of the metamorphism along these belts has been the subject of debate, with proposed ages ranging from Precambrian to Paleozoic (Rossovskiy 1980; Rossovskiy et al. 1982), but recent ^{40}Ar–^{39}Ar and U–Pb dating indicated ages as young as Cenozoic for the metamorphism (Fig. 1; Tapponnier et al. 1990; Schärer et al. 1994; Bertrand et al. 1999; Fraser et al. 2001; Jolivet et al. 2001; Leloup et al. 2001; Barley et al. 2003; Gilley et al. 2003).

Ruby is hosted in marbles that are not appropriate for dating. Direct radiometric dating of ruby is impossible by classical techniques, as it contains essentially no radiogenic elements. To date ruby crystallization, which occurs in the range of temperatures $T \approx 620$–690 °C and pressures $P \approx 2.6$ and 3.3 kbar (1 kbar = 100 MPa; Garnier 2003), it is thus necessary to date syngenetic minerals found as primary solid inclusions or coevally grown with the ruby. Micas and zircons are potentially good candidates for constraining the age of ruby formation. Indeed, the closure temperatures of the ^{40}Ar–^{39}Ar system (Giletti 1974; McDougall and Harrison 1988) and the U–Pb system (Cherniak and Watson 2001) are respectively lower and higher than temperatures for ruby formation. Such an approach was applied successfully in northern Vietnam by dating phlogopite and zircons. Both minerals documented the temporal relationship between high-temperature metamorphism and the cooling history of the Day Nui Con Voi metamorphic belt (Garnier et al. 2002, 2005). This work showed that ruby developed 38 Ma ago when the Red River shear zone was ductily active under peak metamorphic conditions; the ruby-bearing marbles cooled through temperatures appropriate for Ar-retention in phlogopite some 18 Ma later. Indirect dating was also attempted using syngenetic phlogopites associated with ruby in Kashmir. The ages of 16 Ma, which were determined for phlogopites from the Nangimali ruby deposit, recorded Neogene cooling that is linked with the extrusion of the Nanga Parbat massif and correspond to a minimum Miocene age for ruby formation (Pêcher et al. 2002).

With the exception of North Vietnam and Kashmir, the ages of ruby deposits in central and southeast Asia were unknown until now. The purpose of this work is to date the formation of ruby in all economic deposits from Asia and to compare the range of ages obtained with the timing of the thermal events known to have affected the metamorphic belts containing the ruby mineralizations. These ages are also compared with those obtained for emerald deposits in the same tectonic zones in Pakistan and Afghanistan. The aim of this work is to understand the temporal relationship between the Indo-Eurasian collision and the mineralizing episodes responsible for ruby and emerald formation. The Cenozoic ^{40}Ar–^{39}Ar and U/Pb ages found previously are confirmed by the dating done in this work on syngenetic mica and zircon crystals. This result implies the existence of a high-quality gemstone belt running from Afghanistan to Vietnam. Furthermore, the compositions of the parental fluids of ruby are identical in all of the deposits and the formation processes are similar (Garnier 2003). All of these metallogenetic features point towards a unique model of ruby formation during distinct Cenozoic thermal episodes linked to the continental collision between India and Eurasia.

Geological setting of the ruby deposits of central and southeast Asia—mechanisms of formation

Geology

Marble-hosted ruby deposits from central and southeast Asia are contained in metamorphic blocks deformed by major tectonic Cenozoic structures related to Indo-Eurasian collision.

The ruby deposit from Jegdalek in Afghanistan is located in the Western Nuristan Block, in the Indus suture zone, near the city of Sairobi (Fig. 1). The area is composed of a metamorphic basement of assumed Precambrian age (Rossovskiy et al. 1982) intruded by Oligocene (34–26 Ma, Debon et al. 1986) plutonic units that define the southern part of the axial batholith defined by Debon et al. (1986) in the Western Nuristan block. The ruby deposits are hosted by Precambrian marbles (Rossovskiy et al. 1982). The deposits from Batakundi and Nangimali in Azad Kashmir are located in the High Himalaya Crystalline formation, in the southern part of the Nanga Parbat. The Nangimali deposit is situated within a syncline developed during the upper Cretaceous to Miocene Himalayan tectono-metamorphic event (Pêcher et al. 2002). The deposits from Chumar and Ruyil in Nepal are located in the southeastern flank of the Ganesh Himal, in the Nawakot series, just below the MCT. These deposits are found within boudinaged marble lenses, 60–150 m thick and up to 1 km long, striking parallel to the MCT.

Marble-hosted ruby deposits in the Hunza valley (Pakistan), Mogok (Myanmar), and Yen Bai (Vietnam) share many structural and mineralogical features (Hughes 1997). They are hosted by a metamorphosed platformal carbonate sedimentary series made up of marbles intercalated with calc-schists and sillimanite- or kyanite-bearing gneisses. These marble units consist of discontinuous horizons ranging from 0.1 to 300 m thick and subparallel to the main regional structural trend related to the Cenozoic Himalayan orogenesis. These metamorphosed sediments are intruded by dykes of granite and (or) pegmatite. In Luc Yen, Nangimali, and Hunza, amphibolite bodies alternate with calcitic and (or) dolomitic marbles. The assemblage is essentially made up of calcite, dolomite, spinel, phlogopite, margarite, amphibole, chlorite, forsterite, and rutile ± graphite ± garnet ± pyrite. The surrounding gneisses or schists show assemblages of biotite–garnet–sillimanite ± scapolite ± kyanite ± amphibole ± clino-pyroxene.

The deposits from the Hunza Valley in Pakistan are localized in the Baltit metamorphic formation from the Karakoram

metamorphic complex, north of the Nanga Parbat massif, between the main Karakoram thrust and the intrusive Karakoram batholith. The famous Mogok ruby deposits are enclosed in the Mogok metamorphic belt, which is formed by rocks of greenschist to granulite facies (Bender 1983). This belt accommodated a large part of the Indo-Eurasian collision (Bertrand et al. 2001) and is marked by high-grade metamorphic ductile Oligocene stretching and post-Miocene brittle right-lateral faults, such as the Shan scarp fault zone and the Sagaing fault (Bertrand and Rangin 2003). The ruby deposits from Vietnam are located in major shear zones, such as the Red River shear zone in Luc Yen, northern Vietnam, and the Quy Chau shear zone in central Vietnam. These shear zones were active during the Cenozoic (Schärer et al. 1990*a*, 1994; Tapponnier et al. 1990; Jolivet et al. 1999; Maluski et al. 1999).

Three types of ruby-bearing mineralization are described (Garnier 2003): (1) dissemination within marbles in association with phlogopite, margarite, rutile, pyrite, and graphite in Jegdalek, Chumar, Ruyil, Mogok, Mong Hsu, and Luc Yen; (2) veinlets or gash veins, in some occurrences of northern Vietnam, in association with phlogopite, margarite, rutile, and pyrite, and sometimes obviously related to micro-shear zones, as in Nangimali; (3) pockets in association with orthoclase, phlogopite, margarite, and pyrite, in some occurrences of northern Vietnam.

Ruby formation

Petrographic and stable isotope studies (C- and O-isotopic compositions of carbonates enclosing ruby, O-isotopes in corundum, and H-isotopes in micas associated with ruby) have shown that (1) ruby grew in a closed system buffered by metamorphic fluids that were released during the metamorphic devolatilization of carbonates that reacted with evaporites (Garnier 2003; Garnier et al. 2004; Giuliani et al. 2005), and (2) magmatic fluids were not at all involved in the formation of the gemstones. The high $\delta^{18}O$ values of ruby from Asian marble-hosted deposits ($16.9‰ < \delta^{18}O < 23.0‰$) indicated that the ruby oxygen composition was buffered by the host carbonates and confirmed the metamorphic origin of the ruby (Garnier 2003). Giuliani et al. (2003*a*) reported unusual fluid-inclusion chemical compositions, indicating that the parent fluids were evaporitic in origin. These compositions fixed the conditions of gem ruby formation during the retrograde metamorphic path (T = 620–690 °C and P = 2.6–3.3 kbar; Fig. 2), as determined with the TWEEQ software (Berman 1991) and assuming pure end members (spinel, phlogopite, muscovite, margarite, and corundum). The aluminium and the chromophorous elements of ruby (chromium and vanadium) originate from the marbles. The ruby mineralization is restricted to peculiar impure marble horizons that are enriched in detrital minerals (in particular clay minerals), organic matter, and intercalated evaporite layers (salts and sulfate). The S-isotopic composition of anhydrite and the B-isotopic composition of tourmaline, both associated with ruby in Vietnam, Pakistan, and Azad Kashmir, corroborate the participation of marine and nonmarine evaporites in the formation of ruby. All these features lead to the proposal that the marble protoliths were deposited in endorheic environments, such as a lagoon. The presence of evaporite is essential because it allowed for the mobilization of aluminium that is necessary for the crystallization of the corundum. In addition, the melting of evaporites during high-temperature metamorphism freed space for the growth of large crystals with few impurities, thus permitting the development of high-quality rubies. Finally, the preservation of ruby in the metamorphic assemblages implies that their host rocks were exhumed and cooled rapidly, otherwise ruby would have been destabilized in mica.

The petrographic relationships provide evidence that mica (phlogopite, muscovite, and margarite) and spinel reacted to form ruby (Garnier 2003). The genetic link between ruby and phlogopite is shown by the petrographic relationships of the minerals making up the mineralogical assemblages. In addition, phlogopite is found as solid inclusions trapped along growth zones in ruby crystals from all the studied deposits, thus confirming the syngenetic character of both minerals (Giuliani et al. 2003*a*).

In Jegdalek, Nangimali, and deposits from northern Vietnam, muscovite reacted to form ruby and phlogopite following

[1] $$\text{muscovite} + \text{dolomite} \leftrightarrow \text{phlogopite} + 3\ \text{calcite} + \text{corundum} + 3\ CO_2$$

In Nepal, ruby formed following

[2] $$3\ \text{anorthite} + 6\ \text{dolomite} + 2\ H_2O + 2\ KCl \leftrightarrow 2\ \text{phlogopite} + CaCl_2 + 8\ \text{calcite} + 4\ CO_2 + 2\ \text{corundum}$$

Furthermore, the petrography for some Vietnamese samples indicate that ruby formed following

[3] $$30\ \text{anorthite} + 12\ \text{Mg-chlorite} + 10\ K_2O + 6\ CO_2 + 6\ Na_2O + 3\ O_2 \leftrightarrow 12\ \text{pargasite} + 10\ \text{phlogopite} + 6\ \text{calcite} + 32\ \text{corundum} + 64\ H_2O$$

Samples and techniques

The radiometric ^{40}Ar–^{39}Ar stepwise heating method was performed on single grains. The micas were carefully separated by hand picking from marbles and one pegmatite, and cleaned in acetone in an ultrasonic bath. The mica concentrates were analyzed by X-ray diffraction; all the samples showed pure mica spectra without traces of alteration. The diagram of composition Al^{VI} versus X_{Mg} (Fig. 3) shows that all the micas extracted from marbles belong to the phlogopite series, whereas the micas sampled in the Hunza pegmatite are in the field defined by the join annite–siderophyllite. For laser analyses, single grain samples wrapped in pure Al-foil packets were loaded into an irradiation canister with age monitors. Irradiation with fast neutrons was carried out in the McMaster Reactor, Hamilton, Ontario, for 70 h. Age monitors included 520.4 ± 1.7 Ma MMHb hornblende (Alexander et al. 1978) and 24.21 ± 0.32 Ma HD-B1 biotite (Hess and Lippolt 1994). Single-grain ^{40}Ar–^{39}Ar stepwise heating analysis was carried out using a LEXEL 3500 continuous wavelength 6W argon-ion laser. Five argon isotopes were measured using a MAP 215-50 mass spectrometer equipped with a Nier source and a JOHNSTON MM1 electron multiplier at the University of Montpellier, Montpellier,

Fig. 2. *P–T* diagram showing the stability conditions of corundum-micas assemblages in marbles (obtained with the TWEEQ program) and the closure temperature of the ^{40}Ar–^{39}Ar system in phlogopite (Giletti 1974) and U–Pb system in zircon (Cherniak and Watson 2001), which have been applied to the *P–T* conditions of formation for the Vietnamese rubies (Luc Yen district). Grey curve is the *P–T* path for the ruby-bearing rocks, based on geothermometric and microthermometric data (Garnier 2003). An, anorthite; And, andalusite; Cc, calcite; Chl, chlorite; Co, corundum; CO_2, carbon dioxide; Do, dolomite; Dsp, diaspore; Kfs, potash feldspar; Ky, Kyanite; Mrg, margarite; Ms, muscovite; Phl, phlogopite; Si, sillimanite; Sp, spinel; W, water; dsCO_2, isochores for primary fluid inclusions in gem-ruby samples calculated from the density of the carbonic phase (Giuliani et al. 2003*a*).

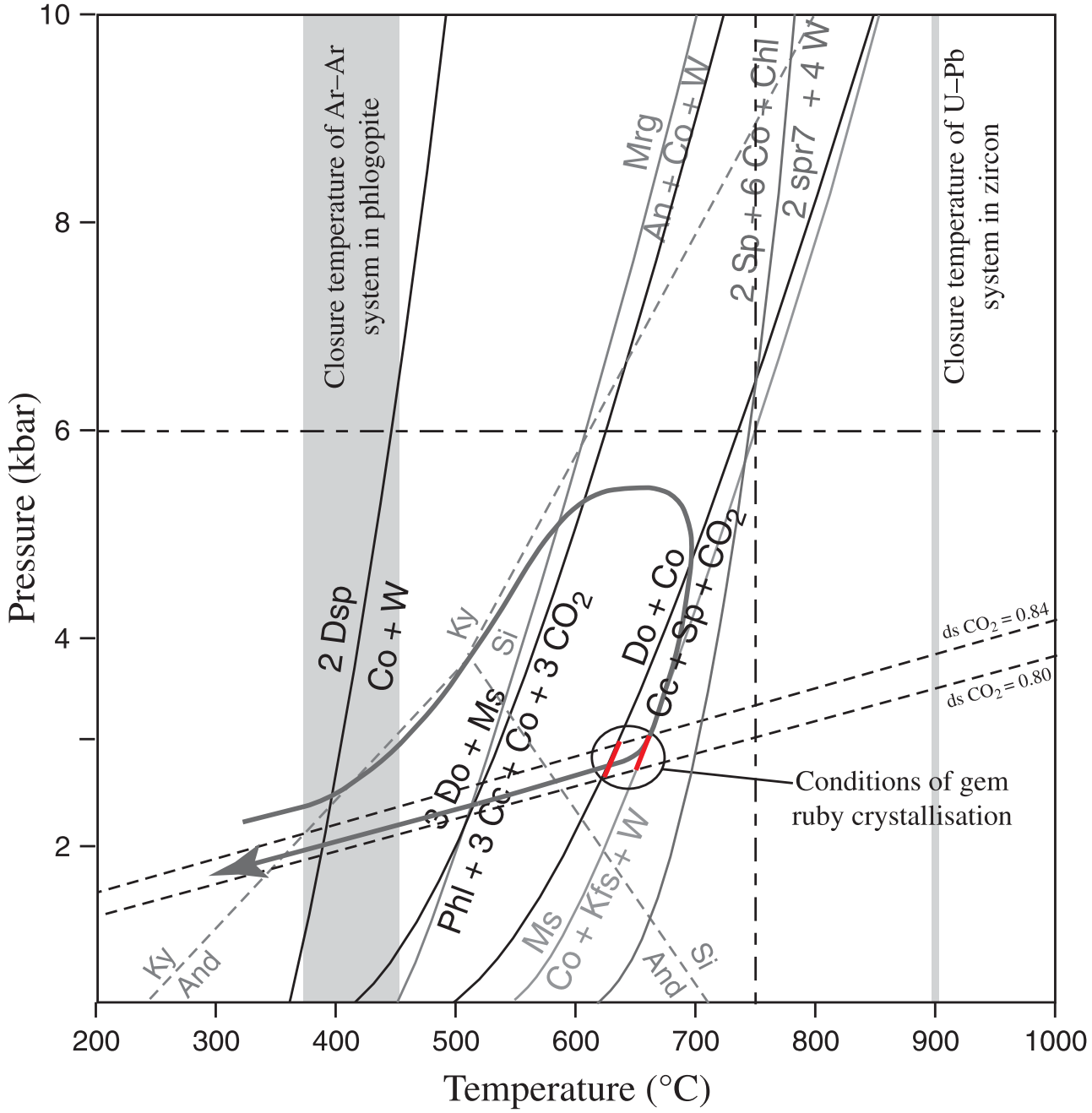

France. Measured Ar isotopes were corrected for blanks, atmospheric contamination, mass discrimination, irradiation-induced Ar isotopes, and radioactive decay of ^{37}Cl and ^{39}Ar. Ages were calculated using constants recommended by Steiger and Jäger (1977) and McDougall and Harrison (1988). Reported errors are 1σ for plateau and total ages, which include analytical uncertainties and age-monitor uncertainties. Errors were calculated following McDougall and Harrison (1988). The strict criteria of a plateau fraction was not defined in this study because all spectra yielded plateaus consisting of > 70% of released argon, corresponding to clustered ages with < 5% variation.

Zircon grains in rubies from Hunza and Quy Chau deposits were imaged by back-scattered electrons with a Hitachi 2500 scanning electron microscope (SEM), as well as by cold cathodoluminescence on a Technosyn apparatus and hot

Fig. 3. Diagram Al^{VI} versus X_{Mg} showing the mineralogy of the dated micas.

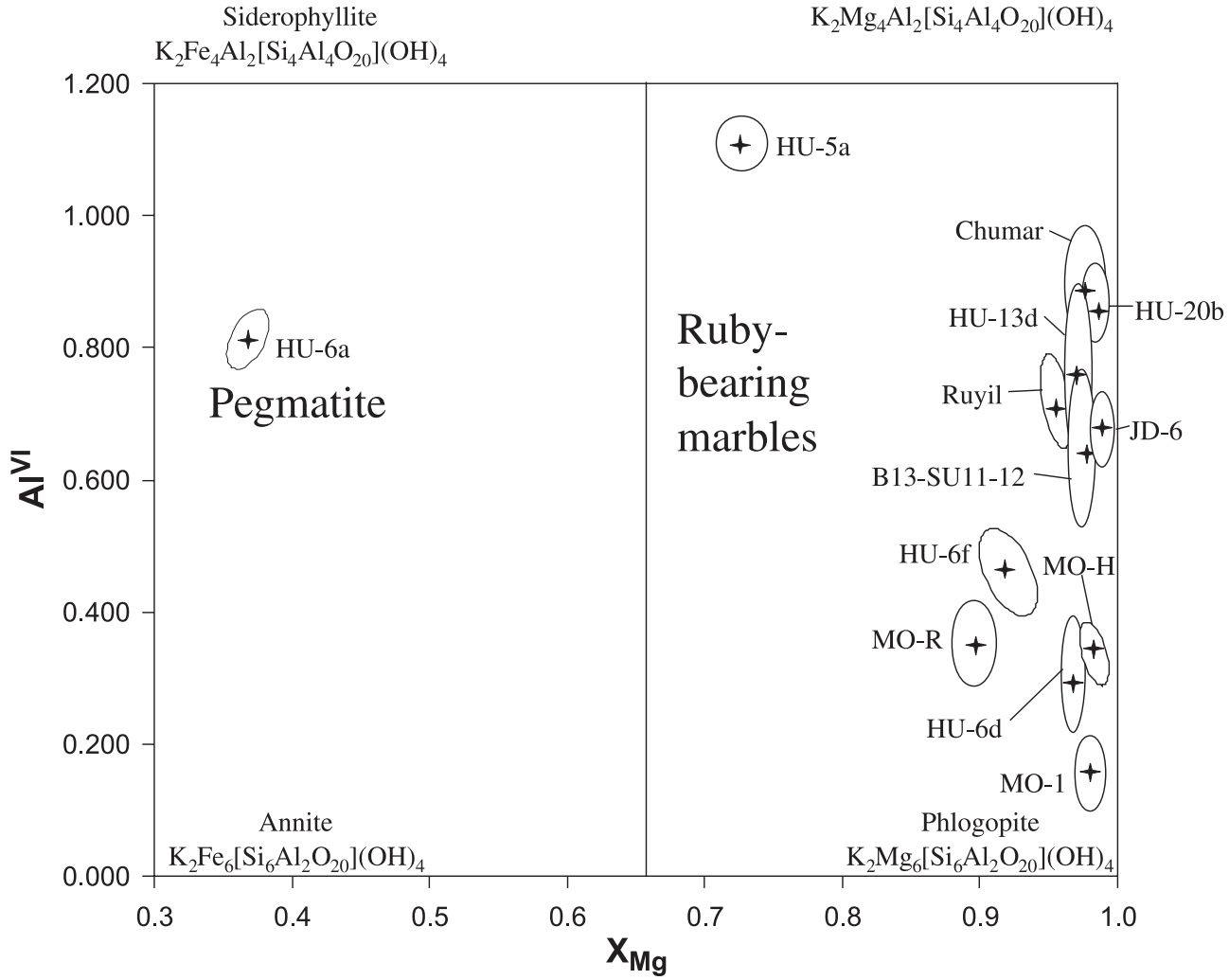

cathodoluminescence on a Philips XL 30 SEM. The U–Pb analyses were performed with a Cameca IMS-1270 ion probe at CRPG-CNRS, Nancy, France. The analytical procedure was detailed in Deloule et al. (2002). The size of the spots varied between 30 × 40 μm^2 and 10 × 20 μm^2. Pieces of the 91500 zircon standard from Kuehl Lake in Renfrew County, Ontario, with an age of 1062.4 ± 0.4 Ma (Wiedenbeck et al. 1995), were mounted with samples and measured every three analyses. The external error from this standard was propagated onto the sample of unknown age. The decay constants of Jaffey et al. (1971) were used to calculate the ages. Corrections for common lead were calculated at the ^{207}Pb–^{206}Pb measured age using the Stacey and Kramers (1975) lead evolution model.

Results and Discussion

A summary of ^{40}Ar–^{39}Ar ages is listed in Figs. 4 and 5 and Tables 1 and 2. All the ^{40}Ar–^{39}Ar and U–Pb isotopic data for analyzed minerals are listed in Tables 3 to 8. None of the ^{40}Ar–^{39}Ar age spectra indicate the presence of an excess argon component or any diffusive argon loss. The release spectra yield plateau ages corresponding to 70%–100% of the total ^{39}Ar released. Some of these spectra are dominated by one large step. This pattern results from the high transparency of phlogopites that released most of their argon during one temperature increment. In all cases where an age spectra can be defined (in all but two samples), this age is similar to the total gas age within experimental uncertainties, confirming the reliability of these plateau ages. The U–Pb ages obtained in the zircon grains included in spinels from Hunza and in most of the zircon crystals recovered from the Quy Chau placers are concordant (Tables 6 to 8). Only one reliable ^{238}U–^{206}Pb age is obtained from one zircon included in a ruby from these placers.

Table 1. Summary of the ^{40}Ar–^{39}Ar ages of the Nangimali ruby deposit, Azad Kashmir.

Locality	Sample number	Rock type	Analyzed mineral	Plateau age (Ma)
Nangimali	LK1a	marble	phlogopite	16.1±0.2
	LK3	marble	phlogopite	15.3±0.1
	LKT1d	marble	phlogopite	17.2±0.2
	LKT10	ruby-bearing marble	phlogopite	16.1±0.5

Note: Table is compiled from Pêcher et al. 2002.

Fig. 4. Summary of the K–Ar and Ar–Ar ages of the Jegdalek ruby deposit and of the different plutonic intrusions dated in the Jegdalek area, Afghanistan.

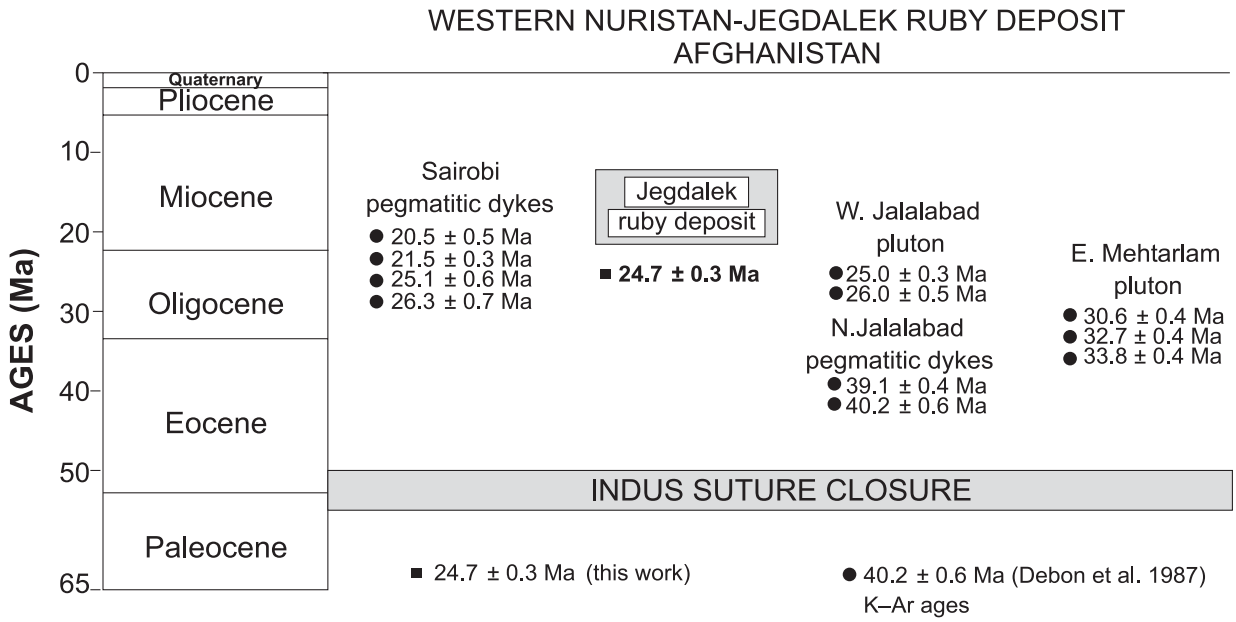

The significance of the Cenozoic ages obtained for all the samples is discussed in the following sections.

Jegdalek, Afghanistan

Micas from the Sairobi pegmatitic dykes recorded K–Ar ages between 26.3 and 20.5 Ma (Debon et al. 1987), which are similar to those from the western part of the aluminous Jalalabad pluton (26.0 ± 0.5 to 25.0 ± 0.3 Ma, Fig. 1). The plateau age of 24.7 ± 0.3 Ma (Fig. 6A) obtained on a phlogopite from the ruby-bearing marble falls within the granite age range. Because of its location relative to the northwestern promontory of the Indian continent, the western Nuristan block suffered a high degree of crustal thickening, which is linked to the subduction of the Indian continental lithosphere beneath Eurasia. This crustal thickening may have triggered the anatexis of continental crust, leading to the formation of aluminous granitoids in the Eocene–Oligocene. Although there is no genetic link between the intrusions and the formation of the ruby mineralizations (see the section on ruby formation earlier in the text), both events are coeval and are also contemporaneous with the emerald deposits in the Panjshir Valley at 23 Ma in Afghanistan (Sabot et al. 2002) and in the Swat Valley in Pakistan at 23.7 Ma (Dilles et al. 1994).

Pakistan and Azad Kashmir

Hunza Valley, Pakistan

^{40}Ar–^{39}Ar dating of micas contained in marble and pegmatite and U–Pb dating of zircon inclusions in spinel from marble provide evidence for two distinct age groups (Figs. 5, 7), as follows:

(1) Three ages between 10.8 ± 0.3 and 9.1 ± 0.3 Ma and one age at 5.4 ± 0.3 Ma were obtained for phlogopite syngenetic with ruby. Additionally, the biotite from a pegmatite located near the ruby deposit of Kharam Butt (Fig. 7) showed evidence of reopening of the isotopic system between 11 and 3 Ma (Figs. 9E–9F) with highly disturbed age spectra. These disturbed age spectra indicate a minimum age of 11.0 ± 0.3 Ma for the thermal event first recorded by these samples, and a maximum age of 3.5 ± 2.0 Ma for the thermal perturbation. These ages are similar to the 11–3 Ma U–Pb monazite ages obtained for the nearby Nanga Parbat region (Zeitler et al. 1993), indicating a Miocene–Pliocene sillimanite metamorphism, which Fraser et al. (2001) relate to dome emplacement and folding along the hanging wall of the Main Karakoram Thrust – Shyok Suture Zone (Fig. 7). These ages are also in agreement with a pulse of uplift evidenced in the Karakoram Baltoro batholith in the eastern part of the Hunza Valley, at the end of the Miocene (Debon et al. 1987; Schärer et al. 1990*b*). The ages obtained on phlogopite indicate that ruby deposits and the Karakoram metamorphic complex crossed the 375–450 °C ^{40}Ar–^{39}Ar closure temperature isotherms during the upper Miocene.

(2) Zircon inclusions in a marble-hosted spinel yielded ages of 93.8 ± 2.1 Ma and 84.6 ± 1.3 Ma respectively. These ages are similar to the lower intercept at 95^{+4}_{-6} defined by Le Fort et al. (1983) for zircon crystals from the Hunza plutonic granodiorite (Fig. 8), which indicate a pre-Indo-Eurasian collisional origin for the Hunza pluton. A ruby-free, phlogopite-bearing marble in the Karakoram metamorphic complex yields an ^{40}Ar–^{39}Ar age of 75.9 ± 1.9 Ma (Fig. 9A). Fraser et al. (2001) reported a U–Pb age of 63.3 ± 0.4 Ma for the sillimanite-bearing pelites intercalated in the Hunza marbles, north of Baltit village (Fig. 7), as well as variable ^{238}U–^{206}Pb ages in the cores of metamorphic monazites ranging from 82.9 ± 6.1 Ma to 61.9 ± 4.7 Ma. The age registered in this ruby-free, phlogopite-bearing marble falls within this range. Fraser et al. (2001) proposed that a pre-collisional metamorphic event occurred more than 60 Ma ago, possibly as long as 80 Ma ago, caused by the collision and accretion of the Kohistan arc to the southern margin of Asia (which

Table 2. Summary of the ^{40}Ar–^{39}Ar ages of the Mogok area.

Locality	Sample number	Rock type	Analyzed mineral	Plateau age (Ma)	Total age (Ma)	Reference
Mogok	MY98-03	Kabaing granite	biotite	15.8±1.1	13.9±1.1	Bertrand et al. 2001
	MY98-MOGOK08		biotite	17.4±0.6	17.5±1.4	Bertrand et al. 2001
	MY98-MOGOK14		biotite	16.5±0.6	16.6±0.6	Bertrand et al. 2001
	MY98-MOGOK15		biotite	19.5±1.0	17.8±0.9	Bertrand et al. 2001
	MO-1	ruby-bearing marble	phlogopite	18.7±0.2	18.8±0.2	This work
	MO-H	marble	phlogopite	17.1±0.2	16.8±0.2	This work
	MO-R	marble	phlogopite	17.9±0.3	17.1±0.3	This work
Northeast	MY98-MOGOK26	granite	biotite	19.1±0.6	18.7±0.6	Bertrand et al. 2001
Mogok	KACHIN11	granite	biotite	15.8±0.7	15.6±0.7	Bertrand et al. 2001

occurred between ca. 102 and 75 Ma) during the Late Cretaceous. This high-grade event may have continued for about 20 Ma after its initiation. Such high-temperature events have also been recorded in zircon inclusions in spinel associated with ruby, as well as in phlogopite from the marbles.

Nangimali, Azad Kashmir

Previous work has shown that micas associated with ruby-bearing and ruby-free-marbles from Nangimali, Nanga Parbat, Himalaya, yielded ^{40}Ar–^{39}Ar age plateaus of 16.1 ± 0.5 Ma and between 17.2 ± 0.2 and 15.3 ± 0.1 Ma, respectively (Table 1). These ages are similar within uncertainty of the ^{40}Ar–^{39}Ar cooling ages of 19 Ma obtained for the Chichi granite (Schneider et al. 1999). However, the (C- and O-) isotopic compositions of the marbles indicate that the marbles acted as a closed system and were not pervasively infiltrated by magmatic fluids, showing that there is no genetic link between the ruby mineralization and the emplacement of this intrusion (Pêcher et al. 2002). These Miocene minimum ages of ruby formation are consistent with those between 20 and 10 Ma that are found in the western and eastern borders of the Nanga Parbat massif, which are interpreted to be probably linked to the vertical extrusion of this massif (Pêcher et al. 2002). The lines of constant cooling ages in the Nanga Parbat were drawn from the ^{40}Ar–^{39}Ar ages obtained on phlogopite and biotite from the ruby deposits, combined with previous published data (see map in Pêcher et al. 2002). They show the extrusion of the central deep-crustal pop-up corner of the massif. Thus in this area, the Early to Middle Miocene metamorphism and anatexis, ubiquitous elsewhere in the Central Himalaya, could also be the dominant thermal event (Pêcher et al. 2002).

Chumar and Ruyil, Nepal

The Ganesh Himal ruby deposits occur in the Lesser Himalaya near the top of the Nawakot series and below the inferred trace of the MCT (Fig. 10). Chumar and Ruyil deposits are located in dolomitic marbles, which are devoid of any intrusion of pegmatite and granite. Ages of phlogopite crystals coeval with rubies define a single phase of cooling in each deposit, dated at 5.6 ± 0.4 Ma and 4.6 ± 0.1 Ma, respectively (Figs. 11A–11B). All these ^{40}Ar–^{39}Ar ages are in agreement with the ^{40}Ar–^{39}Ar ages on muscovite determined by Rai (2001) in the lesser Himalaya, the Kathmandu crystalline, and the Gosainkund crystalline nappes. These cooling ages systematically young from south to north, i.e., 22–14 Ma in the Kathmandu Crystalline Nappe, 16–5 Ma in the Gosaikund Crystalline Nappe, and 12–6 Ma in the Lesser Himalaya. They are interpreted as evidence of Late Miocene MCT activity. The youngest ages of the ruby deposits are consistent with several age data from rocks at similar structural levels in central Nepal (Copeland et al. 1997) and show that these deposits formed in relation with the Late Miocene MCT activity.

Mogok, Myanmar

All the ages obtained for the phlogopite in marbles are Early Miocene and fall between 18.7 ± 0.2 and 17.1 ± 0.2 Ma (Table 2, Figs. 6B–6D). These ages are in agreement with the previous range of Oligocene to Middle Miocene cooling ages as defined by Bertrand et al. (2001) for the different rock units of the Mogok metamorphic belt in the Mogok area and in the northeastern region of Mogok (15.8 ± 0.7 Ma < age < 19.1 ± 0.6 Ma; Table 2, Fig. 12,). These ages have recorded the northward passage of the eastern syntaxis with respect to Indochina, which occurred during the Oligocene to Middle Miocene in the central part of Myanmar, as a result of the Indo-Asian oblique collision. Thus, the rubies from Mogok probably formed during the metamorphic episode linked to this extensional tectonism.

Vietnam

Luc Yen, Yen Bai, Red River shear zone

Garnier et al. (2002) showed that across the Red River shear zone, the phlogopites syngenetic with ruby in marbles from the Day Nui Con Voi range yielded Miocene ^{40}Ar–^{39}Ar cooling ages between 24.4 ± 0.4 and 23.2 ± 0.6 Ma. Garnier et al. (2002) also showed that the ruby deposits from the Lo Gam tectonic zone on the eastern flank of Red River shear zone yielded ^{40}Ar–^{39}Ar cooling ages between 33.8 ± 0.4 and 30.8 ± 1.0 Ma. Furthermore, U–Pb in situ dating of zircon inclusions in a ruby from the Lo Gam zone marbles yielded an age of 38.1 ± 2.0 Ma (Garnier et al. 2005), leading to the following conclusions: (1) ruby formed around 40–36 Ma, during ductile deformation, under peak metamorphic conditions, in the Red River shear zone; and (2) the deformation ended towards 35 Ma in the Lo Gam zone (Garnier et al. 2002). The ruby-bearing marbles cooled rapidly, whereas the high-temperature deformation continued in the Red River shear zone, resulting in cooling through the blocking temperature of the ^{40}Ar–^{39}Ar system some 15 Ma later. The Red River shear zone acted as a sinistral shear zone from 35 to

Table 3. Argon isotopic data for the Mogok mining district ruby deposit in Myanmar and the Jegdalek ruby deposit in Afghanistan.

Steps	$^{40}Ar^*/^{39}Ar$	$^{36}Ar/^{40}Ar$	$^{39}Ar/^{40}Ar$	$^{37}Ar/^{39}Ar$	% Atm	Cumulative % ^{39}Ar	Age ± 1sd (Ma)
MO-1 Phlogopite (J = 0.017791)							
1	0.837±0.22	1.264	0.748	0.058	37.3	0.3	26.7±7.0
2	0.615±0.06	1.683	0.816	0.010	49.7	1.5	19.6±1.8
3	0.610±0.04	0.271	1.506	0.004	8.0	2.8	19.5±1.3
4	0.579±0.03	0.404	1.520	0.002	11.9	6.0	18.5±0.9
5	0.585±0.01	0.170	1.622	0.000	5.0	31.0	18.7±0.2
6	0.586±0.00	0.084	1.664	0.000	2.4	89.5	18.7±0.1
7	0.595±0.02	0.327	1.516	0.000	9.6	97.6	19.0±0.5
8	0.643±0.05	0.191	1.466	0.000	5.6	99.2	20.5±1.7
9	0.653±0.09	0.023	1.520	0.000	0.6	100	20.8±2.7
							Total age = 18.8±0.2
MO-H Phlogopite (J = 0.017791)							
1	0.247±0.19	3.018	0.437	0.149	89.1	0.5	7.9±6.0
2	0.514±0.09	2.494	0.511	0.007	73.7	1.9	16.4±2.9
3	0.499±0.04	1.493	1.118	0.003	44.1	5.0	15.9±1.2
4	0.656±0.06	0.012	1.517	0.000	0.3	7.1	20.9±1.8
5	0.583±0.02	0.431	1.494	0.000	12.7	9.2	18.6±0.6
6	0.573±0.01	0.661	1.404	0.002	19.5	14.9	18.3±0.4
7	0.549±0.02	0.302	1.657	0.002	8.9	18.9	17.5±0.7
8	0.531±0.01	0.579	1.560	0.000	17.1	48.4	16.9±0.2
9	0.527±0.01	0.287	1.736	0.000	8.4	78.5	16.8±0.3
10	0.568±0.02	0.255	1.626	0.002	7.5	81.5	18.1±0.6
11	0.496±0.01	0.417	1.767	0.000	12.3	100	15.8±0.2
							Total age = 16.8±0.2
M0-R Phlogopite (J = 0.017791)							
1	–0.166±1.29	3.472	0.159	1.309	100	0.3	–5.3±41.3
2	0.433±0.05	2.597	0.536	0.040	76.7	6.6	13.8±1.7
3	0.573±0.02	0.830	1.317	0.001	24.5	21.6	18.3±0.7
4	0.552±0.01	0.773	1.397	0.008	22.8	77.0	17.6±0.2
5	0.566±0.03	0.627	1.437	0.003	18.5	91.8	18.1±0.8
6	0.576±0.013	1.174	1.133	0.016	34.7	94.1	18.4±4.1
7	0.419±0.10	1.714	1.175	0.025	50.6	97.3	13.4±3.0
8	0.282±0.24	2.846	0.563	0.017	84.1	98.9	9.0±7.8
9	0.218±0.27	2.918	0.629	0.110	86.2	100	7.0±8.5
							Total age = 17.1±0.3
JD-6 Phlogopite (J = 0.017791)							
1	46.66±64.30	0.235	0.020	0.040	6.9	0	1090±1127
2	4.422±1.46	2.362	0.068	2.728	69.8	0.0	136±43
3	2.901±0.52	1.146	0.228	0.578	33.8	0.3	90.8±16.0
4	1.145±0.12	1.984	0.361	0.011	58.6	1.5	36.4±3.7
5	0.922±0.09	2.583	0.256	0.000	76.3	3.4	29.4±3.0
6	0.770±0.05	1.262	0.814	0.005	37.3	6.4	24.5±1.6
7	0.755±0.04	0.760	1.026	0.002	22.4	10.1	24.1±1.1
8	0.780±0.00	0.249	1.188	0.000	7.3	90.2	24.9±0.1
9	0.722±0.02	0.653	1.117	0.000	19.3	99.3	23.0±0.5
10	0.583±0.18	1.909	0.746	0.010	56.4	99.9	18.6±5.6
							Total age = 25.1±0.2

Note: Atm, atmospheric argon; sd, standard deviation; MO, Mogok mining district ruby deposit; JD, Jegdalek ruby deposit.

Table 4. Argon isotopic data for Hunza ruby deposits in Pakistan.

Steps	$^{40}Ar^*/^{39}Ar$	$^{36}Ar/^{40}Ar$	$^{39}Ar/^{40}Ar$	$^{37}Ar/^{39}Ar$	% Atm	Cumulative % ^{39}Ar	Age ± 1sd (Ma)
HU-5a Phlogopite (*J* = 0.022821)							
1	0.128±0.02	1.926	3.354	0.000	56.91	6.4	5.3±0.8
2	0.151±0.01	0.911	4.848	0.002	26.9	19.9	6.2±0.4
3	0.127 0.01	0.871	5.844	0.009	25.7	31.2	5.2±0.5
4	0.142±0.04	0.378	6.272	0.000	11.2	35.6	5.8±1.7
5	0.124±0.02	0.770	6.249	0.000	22.8	44.8	5.1±0.8
6	0.135±0.01	0.413	6.488	0.000	12.2	66.6	5.5±0.4
7	0.137±0.01	0.391	6.467	0.000	11.5	79.7	5.6±0.6
8	0.132±0.03	0.506	6.466	0.000	14.9	86.5	5.4±1.0
9	0.129±0.02	0.863	5.752	0.000	25.5	91.3	5.3±0.8
10	0.136±0.00	0.001	7.373	0.044	0.0	95.1	5.6±0.1
11	0.125±0.00	0.424	6.972	0.001	12.5	100	5.1±0.1
							Total age = 76.0±2.3
HU-6a Biotite 1 (*J* = 0.022821)							
1	0.763±0.37	3.228	0.060	0.001	95.4	4.3	31.3±14.9
2	0.217±0.02	1.563	2.474	0.009	46.2	66.0	8.9±0.6
3	0.089±0.02	2.198	3.921	0.003	64.9	96.2	3.7±0.8
4	–0.285±0.26	6.220	2.945	0.001	100	99.3	—
5	–1.636±0.62	11.165	1.406	0.006	100	100	—
							Total age = 7.9±0.9
HU-6a Biotite 2 (*J* = 0.022821)							
1	–4.194±3.85	3.495	0.008	0.033	100	0.4	—
2	–7.361±2.97	4.450	0.043	0.019	100	1.2	—
3	–1.05±0.67	4.041	0.185	0.004	100	4.7	—
4	0.085±0.05	2.889	1.712	0.000	85.4	48.9	3.5±1.9
5	0.271±0.06	0.055	3.634	0.000	1.6	73.6	11.1±2.6
6	0.269±0.03	–0.184	3.920	0.311	-5.5	81.4	11.0±2.6
7	–0.310±0.026	5.794	2.300	0.209	100	87.0	—
8	–0.735±0.33	13.975	4.260	0.799	100	93.4	—
9	0.182±0.32	1.007	3.851	0.198	29.8	100	7.5±13.2
HU-6d Phlogopite (*J* = 0.022821)							
1	1.432±1.54	2.495	0.183	0.069	73.7	0.0	58.04±61.4
2	1.795±1.75	2.077	0.215	0.062	61.3	0.0	72.5±69.1
3	0.535±0.27	3.036	0.192	4.597	89.7	0.3	21.9±10.8
4	2.737±0.89	0.026	0.362	3.242	0.7	0.4	109.3±34.3
5	3.231±0.51	0.386	0.274	0.927	11.4	0.6	128.4±19.7
6	1.786±0.34	1.149	0.370	0.010	33.9	0.8	72.1±13.4
7	2.191±0.07	0.554	0.382	0.854	16.3	3.0	88.0±2.7
8	2.107±0.04	0.294	0.433	0.001	8.7	4.3	84.7±1.4
9	1.796±0.02	0.162	0.530	0.000	4.7	31.5	72.5±0.7
10	1.912±0.01	0.097	0.508	0.000	2.8	99.8	77.1±0.2
11	0.794±0.60	2.711	0.250	0.017	80.1	100	32.4±24.2
							Total age = 76.0±2.3
HU-6f Phlogopite (*J* = 0.022821)							
1	1.332±1.10	2.265	0.248	0.028	66.9	0.0	54.0±43.7
2	0.753±0.23	1.210	0.852	0.006	35.7	0.2	30.8±9.4
3	0.849±0.16	2.075	0.455	0.002	61.3	0.8	34.6±6.3
4	0.261±0.01	2.276	1.251	0.101	67.2	5.9	10.7±0.6
5	0.258±0.01	1.065	2.650	0.000	31.4	9.7	10.6±0.4

Table 4 (*concluded*).

Steps	$^{40}Ar^*/^{39}Ar$	$^{36}Ar/^{40}Ar$	$^{39}Ar/^{40}Ar$	$^{37}Ar/^{39}Ar$	% Atm	Cumulative % ^{39}Ar	Age ± 1sd (Ma)
HU-6f Phlogopite (*J* = 0.022821)							
6	0.263±0.009	0.320	3.432	0.000	9.4	100.0	10.8±0.1
							Total age = 11.0±0.3
HU-13a Phlogopite (*J* = 0.022821)							
1	0.888±0.36	2.933	0.150	0.964	86.6	0.3	36.2±14.3
2	0.077±0.05	3.273	0.425	0.001	96.7	2.0	3.2±2.0
3	0.240±0.02	3.030	0.435	0.145	89.5	8.9	9.8±0.7
4	0.221±0.009	0.727	3.541	0.001	21.5	96.5	9.1±0.1
5	0.216±0.05	0.628	3.755	0.238	18.5	99	8.9±2.2
6	0.145±0.10	1.685	3.454	0.248	49.8	100.0	5.9±4.1
							Total age = 9.1±0.3
HU-20b Phlogopite (*J* = 0.022821)							
1	6.978±4.53	2.857	0.022	9.419	84.4	0	266±161
2	0.294±0.38	3.221	0.163	1.261	95.1	0.1	12.1±15.4
3	0.193±0.15	3.124	0.396	0.005	92.3	0.3	7.9±6.0
4	0.249±0.16	3.178	0.244	0.002	93.9	0.7	10.2±6.5
5	0.299±0.10	2.985	0.394	0.002	88.2	1.1	12.3±4.3
6	0.297±0.05	2.674	0.706	0.048	79.0	2.5	12.2±1.9
7	0.257±0.009	1.285	2.408	0.000	37.9	20.3	10.6±0.1
8	0.255±0.01	0.596	3.224	0.003	17.6	100	10.5±0.5
							Total age = 10.5±0.5

Note: Atm, atmospheric argon; sd, standard deviation; HU, Hunza ruby deposit.

Table 5. Argon isotopic data for Nepal.

Steps	$^{40}Ar^*/^{39}Ar$	$^{36}Ar/^{40}Ar$	$^{39}Ar/^{40}Ar$	$^{37}Ar/^{39}Ar$	% Atm	Cumulative % ^{39}Ar	Age ± 1sd (Ma)
Ruyil Phlogopite (*J* = 0.022821)							
1	–0.172±0.17	3.742	0.613	0.423	100	0.3	–7.1±6.8
2	0.063±0.10	2.752	2.977	0.000	81.3	0.7	2.6±4.3
3	0.237±0.01	0.083	4.117	0.001	2.5	0.9	9.7±0.5
4	0.129±0.12	0.798	5.907	0.060	23.6	2.6	5.3±4.7
5	0.109±0.00	0.491	7.812	0.002	14.5	23.7	4.5±0.1
6	0.114±0.00	0.210	8.234	0.002	6.2	85.9	4.7±0.0
7	0.107±0.00	0.751	7.292	0.010	22.2	98.2	4.4±0.1
8	0.081±0.03	1.607	6.454	0.025	47.5	100	3.3±1.2
							Total age = 4.6±0.2
Chumar Phlogopite (*J* = 0.022821)							
1	78.67±65.84	1.656	0.006	13.38	48.9	0.0	—
2	1.588±2.03	3.317	0.012	0.912	98.0	0.1	64.2±80.5
3	1.772±0.84	3.157	0.038	0.003	93.3	0.3	71.5±33.2
4	0.709±0.22	2.585	0.333	0.302	76.4	0.9	28.9±8.7
5	0.755±0.16	2.766	0.242	0.058	81.7	2.1	30.8±6.4
6	0.209±0.12	3.163	0.314	0.047	93.5	5.9	8.5±4.8
7	0.242±0.06	3.007	0.461	0.075	88.8	11.1	9.9±2.6
8	0.156±0.03	2.866	0.983	0.038	84.7	17.1	6.4±1.3
9	0.118±0.03	2.985	1.003	0.000	88.2	31.0	4.8±1.0
10	0.108±0.05	2.666	1.959	0.000	78.8	35.4	4.4±2.2
11	0.149±0.02	2.263	2.224	0.000	66.9	59.4	6.1±0.8
12	0.137±0.00	1.088	4.955	0.000	32.1	100	5.6±0.1
							Total age = 6.7±0.5

Note: Atm, atmospheric argon; sd, standard deviation.

Table 6. U–Pb isotopic data for zircon inclusions in a spinel from Hunza marble in Pakistan.

Sample	Contents (ppm)			Measured	Corrected ratios					Ages (Ma)			
Furandar	Pb	U	Th	$\frac{^{206}Pb}{^{204}Pb}$	$\frac{^{207}Pb}{^{206}Pb}$	σ	$\frac{^{206}Pb}{^{238}U}$	σ	$\frac{^{207}Pb}{^{235}U}$	σ	$\frac{^{206}Pb}{^{238}U}$	σ	$\frac{^{207}Pb}{^{235}U}$	σ
FD-1.ais	3	266	68	1606	0.04640	0.02334	0.01321	0.01586	0.08450	0.02822	84.6	1.3	82.4	2.2
FD-2.ais	2	168	54	488	0.04811	0.13128	0.01466	0.02261	0.09725	0.13321	93.8	2.1	94.2	11.9

17 Ma (Leloup et al. 1993, 1995; Schärer et al. 1994; Harrison et al. 1996) and maybe prior to 36 Ma (Leloup et al. 2001). The formation of ruby hosted by marble in the Red River area is thus linked with the Tertiary tectonic activity of the Red River shear zone, which accommodated a large part of Indo-Asian convergence immediately following the onset of collision (Harrison et al. 1996).

Quy Chau shear zone

The Quy Chau shear zone is occupied by the Bu Khang dome, which consists of a broad antiform of Paleozoic and Mesozoic sedimentary and metasedimentary rocks overlying a core of micaschists, granitoids, paragneisses, and orthogneisses (Jolivet et al. 1999). The northeastern part of the dome is limited by the major extensional shear zone of Quy Chau. Zircon crystals recovered from Quy Chau alluvial placers and originating from different protoliths show complex growth zoning (Fig. 13), usually with an inner core surrounded by several growth zones. The zircon crystals were not transported because the foliations of their host rocks are preserved in the alluvial placers. Thirty-five of the 52 measured ages are concordant and correspond to analytical spots located in distinct growth zones. The ^{238}U–^{206}Pb ages range between 765.4 and 27.1 Ma (Tables 7, 8). The concordant ^{238}U–^{206}Pb and ^{235}U–^{207}Pb ages range between 260.6 ± 5.5 and 27.1 ± 0.7 Ma. We interpret these ages in the following manner: (1) the age 260.6 ± 5.5 Ma is clearly related to the Indosinian metamorphism (Lepvrier et al. 1997) and (2) the other U–Pb ages, clustering between 33.4 ± 0.5 and 27.0 ± 0.7 Ma, are related to Oligocene events, such as the end of the extension of the Bu Khang dome.

Phlogopites from the Quy Chau marbles within the Quy Chau shear zone yielded ^{40}Ar–^{39}Ar cooling ages of 22.1 ± 0.6 and 21.6 ± 0.6 Ma (Garnier et al. 2002). Thus, the youngest U–Pb and ^{40}Ar–^{39}Ar ages are in agreement with the timing defined for the major extension and exhumation phase of the Bu Khang Dome as dated by ^{40}Ar–^{39}Ar on micas between 36 Ma in the core of the dome and 21 Ma in the northern shear zone which bounds the dome (Lepvrier et al. 1997; Maluski et al. 1999; Jolivet et al. 1999, 2001).

In situ dating of zircon inclusions in rubies from Quy Chau placer yielded only one ^{238}U–^{206}Pb age of 53.8 ± 4.6 Ma (Fig. 14) owing to the low lead content and the high proportion of common lead in the inclusions. This zircon may be inherited or syngenetic with the ruby. Thus, the 53.8 ± 4.6 Ma U–Pb age corresponds to a maximum age for ruby crystallization.

The age or the range of ages for ruby formation is difficult to assess directly. Nevertheless, there is clear evidence that the oxygen isotopic compositions of the rubies were buffered by marbles (Giuliani et al. 2003*b*). This implies that the genesis of ruby is not linked to the plutonism that provoked the formation of a magnesian skarn in the Quy Chau shear zone (Garnier 2003), but rather to a metamorphic episode that must have occurred prior to the emplacement of the granitic intrusions 26.0 Ma ago (Jolivet et al. 2001). Furthermore, Jolivet et al. (2001) have emphasized that the age of the high-pressure episode is not precisely constrained; the ^{40}Ar–^{39}Ar dates indicate that the isotopic closure of the high-pressure micas occurred at 36–33 Ma and that progressive crystallization of younger micas occurred during the exhu-

Table 7. U–Pb isotopic data for the dating of the zircon crystals from the placer of Mo Coi (MC) in the Quy Chau shear zone and of a zircon included in a ruby (QC3), Vietnam.

Sample	Contents (ppm)			Measured	Corrected ratios						Ages (Ma)			
	Pb	U	Th	$\frac{^{206}Pb}{^{204}Pb}$	$\frac{^{207}Pb}{^{206}Pb}$	σ	$\frac{^{206}Pb}{^{238}U}$	σ	$\frac{^{207}Pb}{^{235}U}$	σ	$\frac{^{206}Pb}{^{238}U}$	σ	$\frac{^{207}Pb}{^{235}U}$	σ
MC10.4-pt1	6	1609	152	4341	0.04666	0.01375	0.00470	0.00015	0.03024	0.00104	**30.2**	**0.9**	**30.2**	**1.0**
MC10.4-pt2	7	1848	160	5748	0.04713	0.01748	0.00471	0.00018	0.03060	0.00127	**30.3**	**1.1**	**30.6**	**1.3**
MC10.4-pt3	5	1279	87	7591	0.04877	0.01808	0.00469	0.00014	0.03156	0.00113	**30.2**	**0.9**	**31.6**	**1.1**
MC10.6-pt1	6	1572	88	3820	0.04818	0.03530	0.00474	0.00020	0.03151	0.00171	**30.5**	**1.3**	**31.5**	**1.7**
MC10.6-pt2	7	1551	82	4044	0.04726	0.02138	0.00513	0.00026	0.03341	0.00181	**33.0**	**1.6**	**33.4**	**1.8**
MC1.3-pt1	8	1645	94	5716	0.04600	0.01974	0.00593	0.00015	0.03758	0.00120	38.1	1.0	37.5	1.2
MC1.3-pt2	2	567	40	5814	0.04925	0.02084	0.00491	0.00015	0.03335	0.00125	31.6	1.0	33.3	1.2
MC2.4-pt1	14	435	155	23711	0.05107	0.00789	0.03775	0.00086	0.26581	0.00642	**238.9**	**5.3**	**239.3**	**5.1**
MC2.4-pt2	8	1461	43	15133	0.04938	0.01540	0.00668	0.00020	0.04546	0.00153	**42.9**	**1.3**	**45.1**	**1.5**
MC3.9-pt1	3	109	133	4492	0.05101	0.02804	0.03548	0.00130	0.24955	0.01152	**224.8**	**8.1**	**226.2**	**9.3**
MC3.9-pt2	20	625	115	30177	0.05019	0.00688	0.03804	0.00111	0.26326	0.00791	**240.7**	**6.9**	**237.3**	**6.3**
MC4.7-pt1	14	454	217	31247	0.05064	0.00683	0.03503	0.00126	0.24459	0.00896	**222.0**	**7.8**	**222.2**	**7.3**
MC4.7-pt2	9	288	146	19234	0.05180	0.00718	0.03436	0.00084	0.24535	0.00626	**217.7**	**5.2**	**222.8**	**5.1**
MC6.6-pt1	3	763	68	6555	0.04927	0.02203	0.00443	0.00011	0.03007	0.00102	**28.5**	**0.7**	**30.1**	**1.0**
MC6.6-pt2	2	585	62	8015	0.05030	0.02648	0.00482	0.00016	0.03345	0.00140	31.0	1.0	33.4	1.4
MC6.6-pt3	5	1355	167	8759	0.04812	0.01194	0.00421	0.00011	0.02791	0.00079	**27.1**	**0.7**	**27.9**	**0.8**
MC7.2-pt1	3	757	65	5249	0.04616	0.01293	0.00482	0.00010	0.03070	0.00077	**31.0**	**0.7**	**30.7**	**0.8**
MC7.2-pt2	5	1226	73	28265	0.04779	0.00736	0.00506	0.00010	0.03333	0.00070	**32.5**	**0.6**	**33.3**	**0.7**
MC7.3-pt1	3	855	13	4269	0.04745	0.02138	0.00471	0.00014	0.03083	0.00112	**30.3**	**0.9**	**30.8**	**1.1**
MC7.3-pt2	4	952	16	4478	0.04791	0.02403	0.00481	0.00019	0.03178	0.00144	**30.9**	**1.2**	**31.8**	**1.4**
MC8.1-pt1	6	183	129	1343	0.05882	0.06379	0.03657	0.00168	0.29660	0.02332	231.6	10.4	263.7	18.1
MC8.1-pt2	65	1831	78	28318	0.05099	0.00626	0.04125	0.00089	0.28999	0.00654	**260.6**	**5.5**	**258.6**	**5.1**
MC9.1-pt1	195	1804	118	64334	0.06911	0.03240	0.12607	0.00625	1.20133	0.07114	**765.4**	**35.7**	**801.2**	**32.3**
MC9.10-pt1	14	476	45	6168	0.05063	0.01335	0.03386	0.00085	0.23635	0.00675	**214.6**	**5.3**	**215.4**	**5.5**
MC9.10-pt2	3	825	111	2906	0.04368	0.04809	0.00443	0.00010	0.02668	0.00142	**28.5**	**0.7**	**26.7**	**1.4**
MC9.10-pt3	4	922	73	1903	0.04556	0.03476	0.00561	0.00013	0.03522	0.00146	**36.0**	**0.8**	**35.1**	**1.4**
QC3	6	899	95	49			0.00838	0.00072			53.8	4.6		

Note: Bolded numbers indicate concordant ages.

Table 8. U–Pb isotopic data for the dating of the zircon crystals from the placer of Bai Trieu in the Quy Chau shear zone, Vietnam.

Sample	Contents (ppm)			Measured	Corrected ratios						Ages (Ma)			
	Pb	U	Th	$^{206}Pb/^{204}Pb$	$^{207}Pb/^{206}Pb$	σ	$^{206}Pb/^{238}U$	σ	$^{207}Pb/^{235}U$	σ	$^{206}Pb/^{238}U$	σ	$^{207}Pb/^{235}U$	σ
NA-10.4pt1	15	546	20	26085	0.05102	0.00441	0.22390	0.00252	0.03183	0.00033	**202.0**	**2.1**	**205.2**	**2.1**
NA-10.4pt2	13	2062	8	27196	0.04728	0.00864	0.04739	0.00066	0.00727	0.00008	**46.7**	**0.5**	**47.0**	**0.6**
NA-10.4pt3	3	784	26	261	0.03513	0.24772	0.02228	0.00575	0.00460	0.00033	29.6	2.1	22.4	5.7
NA-3.10pt1	35	4967	8	107148	0.04765	0.00520	0.05434	0.00065	0.00827	0.00009	**53.1**	**0.6**	**53.7**	**0.6**
NA-3.10pt2	27	3824	6	4783	0.04646	0.01332	0.05299	0.00099	0.00827	0.00011	**53.1**	**0.7**	**52.4**	**1.0**
NA-3.7pt1	12	2064	5	17221	0.04769	0.00923	0.04632	0.00065	0.00704	0.00007	**45.3**	**0.5**	**46.0**	**0.6**
NA-3.7pt2	18	2968	8	3252	0.04709	0.02256	0.04514	0.00161	0.00695	0.00019	**44.7**	**1.2**	**44.8**	**1.6**
NA-3.7pt3	12	2196	5	2739	0.04592	0.02222	0.04193	0.00166	0.00662	0.00022	**42.6**	**1.4**	**41.7**	**1.6**
NA-4.10pt1	3	578	19	7803	0.04646	0.01212	0.03281	0.00054	0.00512	0.00006	**32.9**	**0.4**	**32.8**	**0.5**
NA-4.10pt2	4	803	25	4471	0.04186	0.01565	0.03034	0.00060	0.00526	0.00006	33.8	0.4	30.3	0.6
NA-4.10pt3	5	1064	32	6403	0.04561	0.00683	0.03335	0.00044	0.00530	0.00006	34.1	0.4	33.3	0.4
NA-4.10pt4	3	710	19	9551	0.04666	0.01495	0.03337	0.00068	0.00519	0.00007	**33.4**	**0.5**	**33.3**	**0.7**
NA-4.3pt1	5	743	16	12561	0.04617	0.00779	0.05085	0.00068	0.00799	0.00009	**51.3**	**0.6**	**50.4**	**0.7**
NA-4.3pt2	15	474	360	35778	0.06167	0.12868	0.31564	0.04080	0.03712	0.00045	235.0	2.8	278.5	31.0
NA-4.3pt3	41	4030	62	70398	0.04793	0.00524	0.07814	0.00114	0.01182	0.00016	**75.8**	**1.0**	**76.4**	**1.1**
NA-6.2pt1	8	1605	10	12593	0.04657	0.01253	0.03740	0.00063	0.00582	0.00006	**37.4**	**0.4**	**37.3**	**0.6**
NA-6.2pt2	6	781	3	774	0.04616	0.08345	0.05340	0.00454	0.00839	0.00014	**53.9**	**0.9**	**52.8**	**4.4**
NA-6.8pt1	6	1299	68	9430	0.04239	0.01351	0.03092	0.00074	0.00529	0.00010	34.0	0.7	30.9	0.7
NA-6.8pt2	3	639	38	5887	0.04314	0.01800	0.03121	0.00065	0.00525	0.00006	33.7	0.4	31.2	0.6
NA-8.6pt1	3	446	4	4945	0.04548	0.01288	0.05141	0.00087	0.00820	0.00009	52.6	0.6	50.9	0.8
NA-8.6pt2	2	395	27	6845	0.03292	0.02635	0.02268	0.00066	0.00500	0.00006	32.1	0.4	22.8	0.7
NA-8.6pt3	3	548	12	3970	0.03981	0.01740	0.02974	0.00067	0.00542	0.00008	34.8	0.5	29.8	0.7
NA-9.2pt1	3	648	11	3313	0.04681	0.02865	0.03562	0.00110	0.00552	0.00006	**35.5**	**0.4**	**35.5**	**1.1**
NA-9.2pt2	1	213	19	2334	0.04062	0.04368	0.02899	0.00132	0.00518	0.00007	33.3	0.4	29.0	1.3

Note: Bolded numbers indicate concordant ages.

Fig. 5. Summary of the Rb–Sr, K–Ar, Ar–Ar and U–Pb ages of the Hunza ruby-bearing marbles and of the various plutonic intrusions from the Hunza Valley, Pakistan.

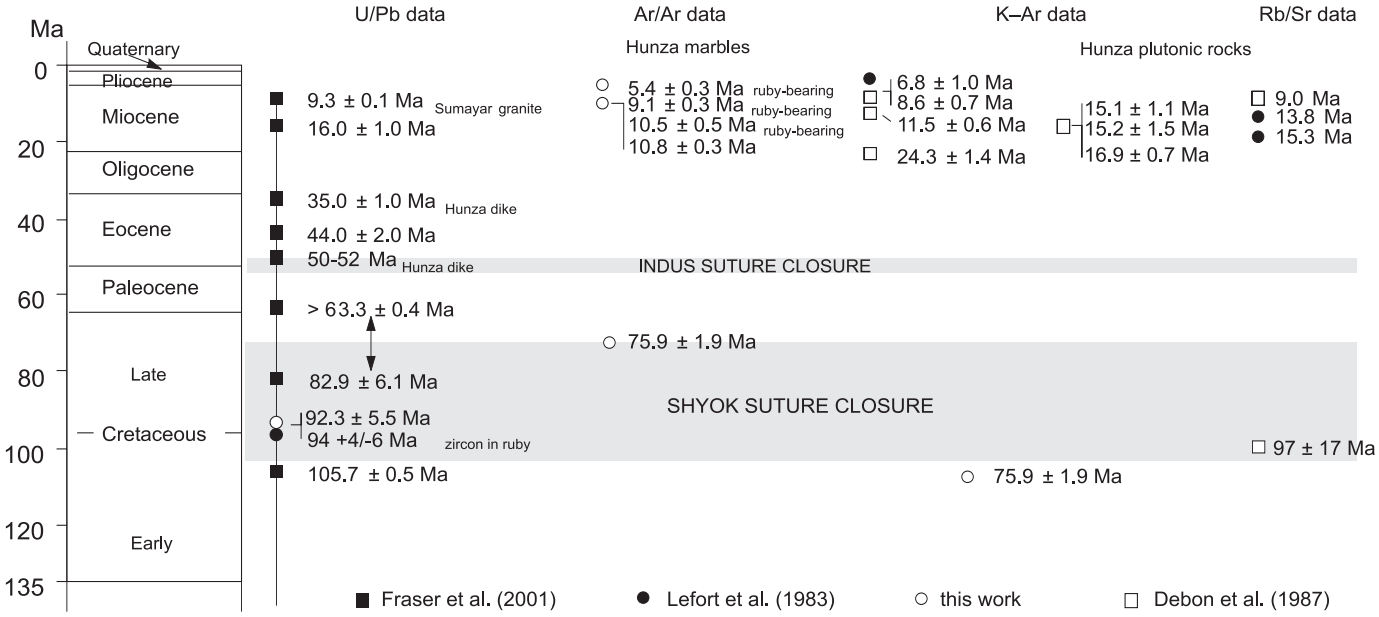

Fig. 6. ^{40}Ar–^{39}Ar age spectra of phlogopite samples from the (A) Jegdalek, Afghanistan and (B–D) the Mogok, Myanmar, ruby deposits. Ar–Ar plateau ages are reported, Arrows indicate the extent of the Ar–Ar plateau.

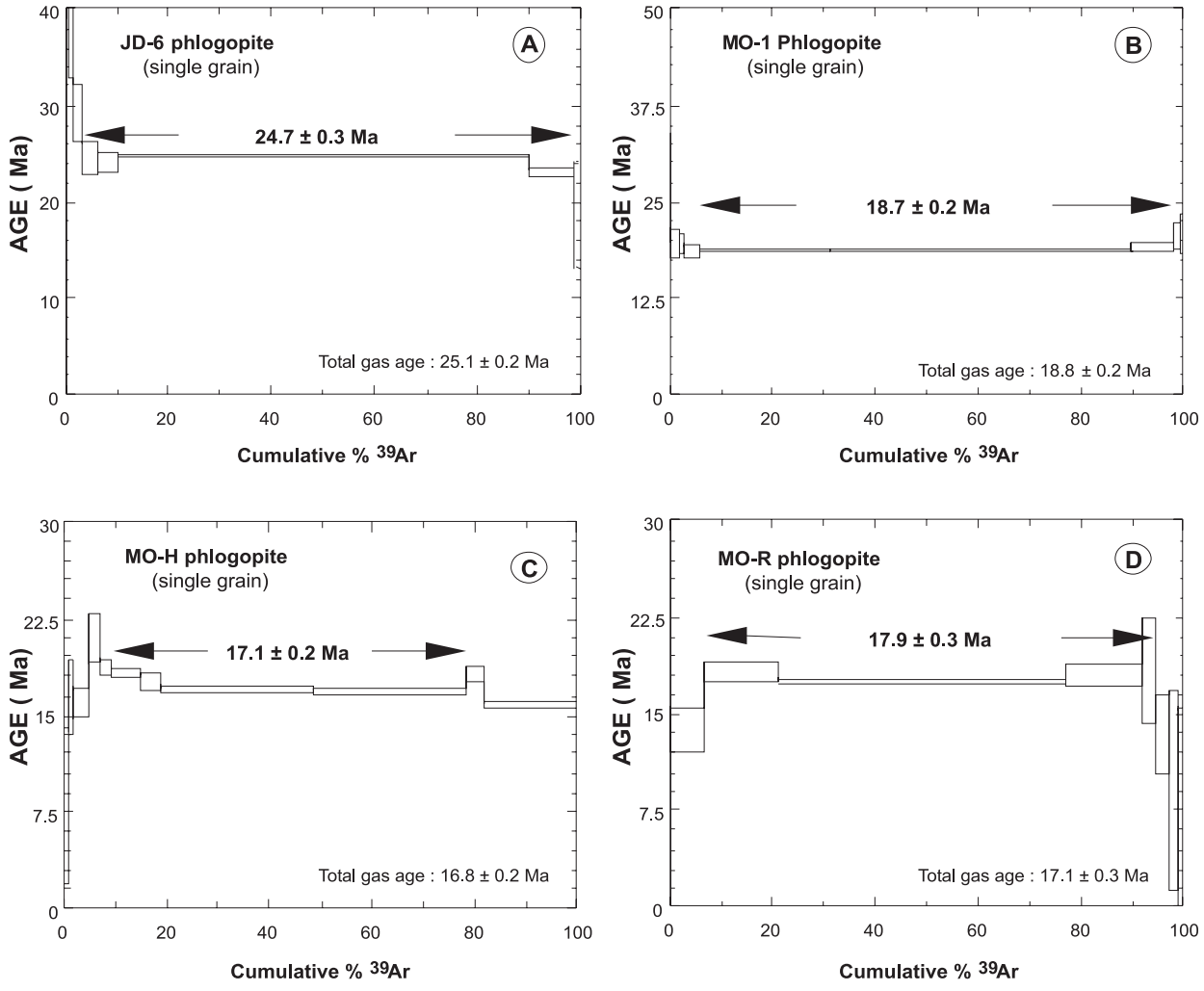

Fig. 7. Geological map from the Hunza Valley, Pakistan (modified after Khan et al. 1987; Crawford and Searle 1993). 1, road; 2, river; 3, glacier; 4, ruby occurrence; 5, fault and thrust; 6, regional dip; 7, gneisses, schists, and ruby-bearing marbles; 8, schists and quartzites; 9, aplites and pegmatites; 10, Hunza plutonic complex; 11, Nagar leucogranite; 12, eluvium and colluvium.

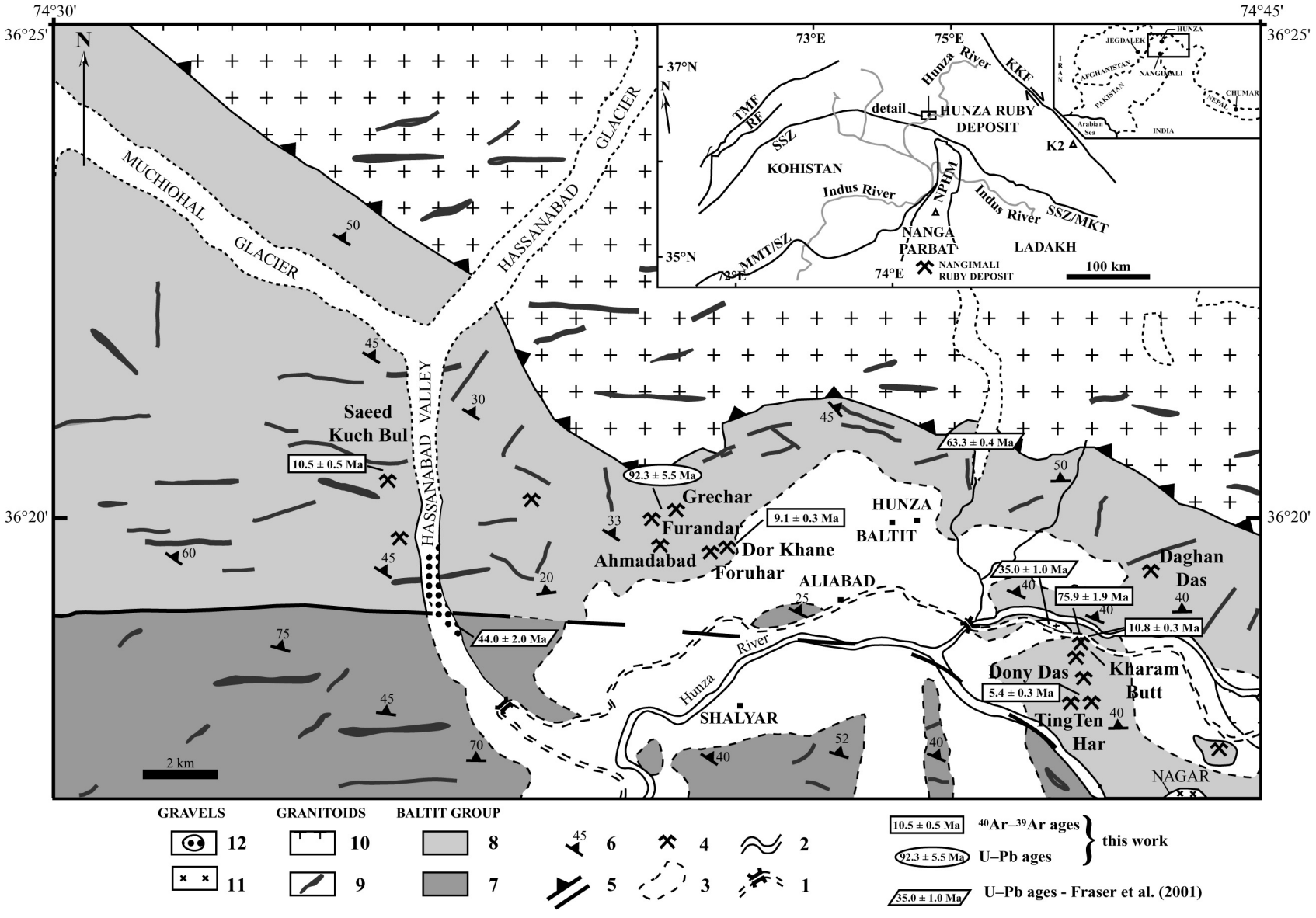

Fig. 8. Wetherill diagram obtained for the zircon inclusions in a spinel from the Furandar deposit in the Hunza Valley, Pakistan. Data is from Le Fort et al. (1983), Fraser et al. (2001), and this study.

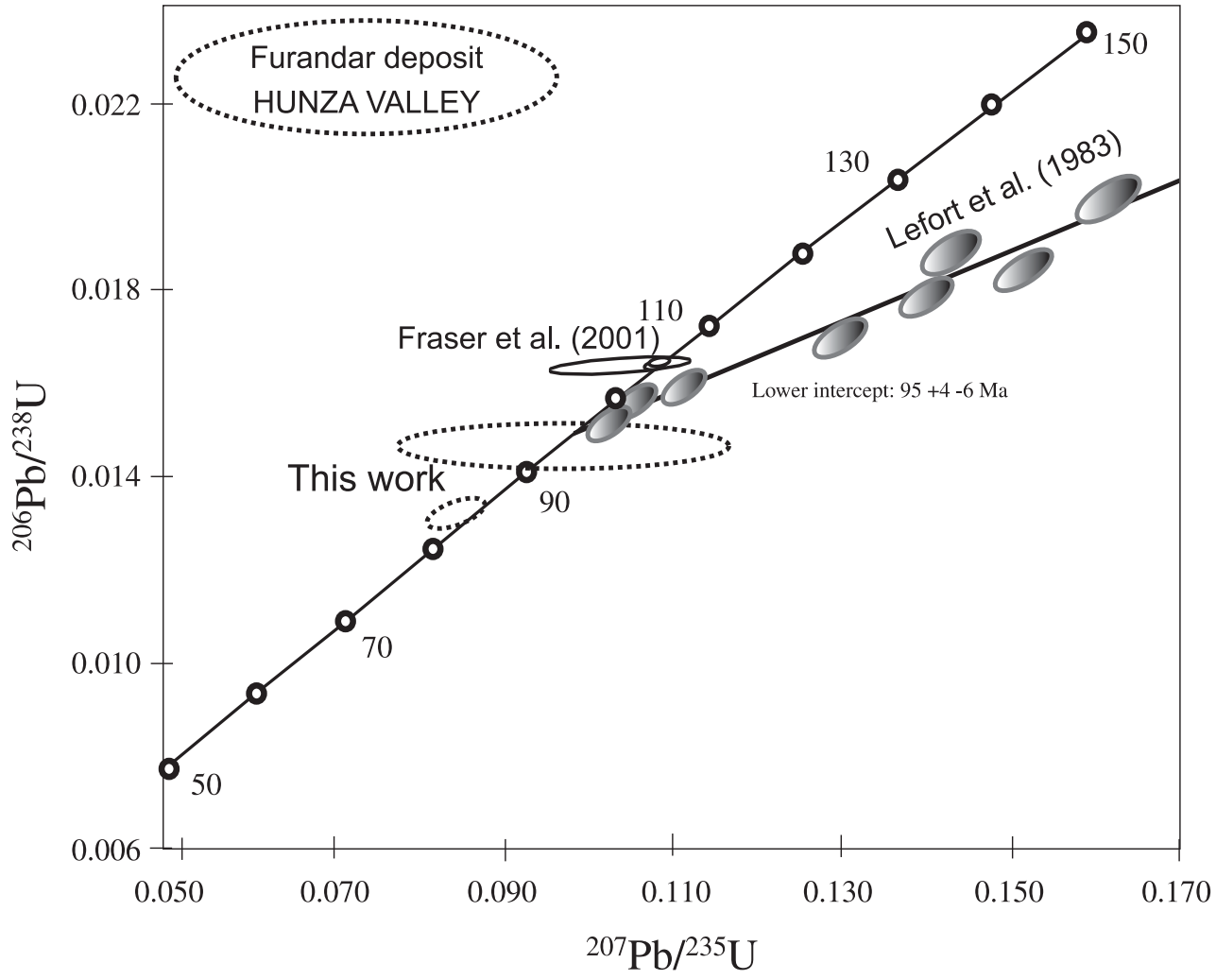

mation and the localization of shear along the major shear zone. Jolivet et al. (2001) proposed that the high-pressure metamorphic episode inside the dome was probably of Oligocene age.

In the Red River shear zone as well as in the Jegdalek and Hunza deposits, gem-quality ruby formed during the retrograde metamorphic path ($400 < T < 600$ °C; $2 < P < 6$ kbar; Garnier 2003). Assuming that ruby formed under the same conditions in Quy Chau, the crystallization of ruby began during the high-pressure metamorphic episode, i.e., before 36–33 Ma (and maybe already at 54 Ma), and may have lasted until 22–21 Ma under low *P*–*T* metamorphic conditions.

Conclusions

(1) New ^{40}Ar–^{39}Ar and U–Pb ages from phlogopite-bearing marbles and zircon-bearing rubies address the crystallization and metamorphic history of the ruby deposits in central and southeast Asia. The ruby is of metamorphic origin. The ^{40}Ar–^{39}Ar data presented in this paper document Oligocene–Miocene cooling ages for the ruby-bearing metamorphic belts, which represent minimum ages for ruby formation. U–Pb in situ dating of zircon inclusions in Vietnamese ruby gives a maximum Eocene age for ruby crystallization for the Luc Yen and Quy Chau deposits. The formation of ruby is strictly associated with the high-temperature metamorphism of the Himalayan fold belt which developed during the Tertiary collision of the Indian subcontinent northward into Asia.

(2) The ^{40}Ar–^{39}Ar data obtained in this study are in agreement with the tectono-metamorphic history of the formations containing the ruby mineralizations and documented elsewhere in the literature. The formation of the Jegdalek deposit occurred in the Oligocene. Similar ages were inferred for the Quy Chau deposit, which formed during the extension of the Bu Khang dome that is related to the opening of the South China sea and for the Lo Gam zone in northern Vietnam. The ruby deposits from Jegdalek are coeval with the emerald deposits from the Panjshir Valley in Afghanistan and from the Swat Valley in Pakistan. In Hunza in the Karakoram metamorphic complex and in the Day Nui Con Voi range in northern Vietnam, ruby formation occurred in the Late Miocene. The Nangimali deposit in Pakistan yields Early Miocene

Fig. 9. ^{40}Ar–^{39}Ar age spectra of micas from the Hunza Valley in the Karakoram mountains, Pakistan. (A) Ruby-free marble. (B–D, G) Ruby-bearing marbles. (E, F) Biotite from one pegmatite. Ar–Ar plateau ages are reported. Arrows indicate the extent of the Ar–Ar plateau.

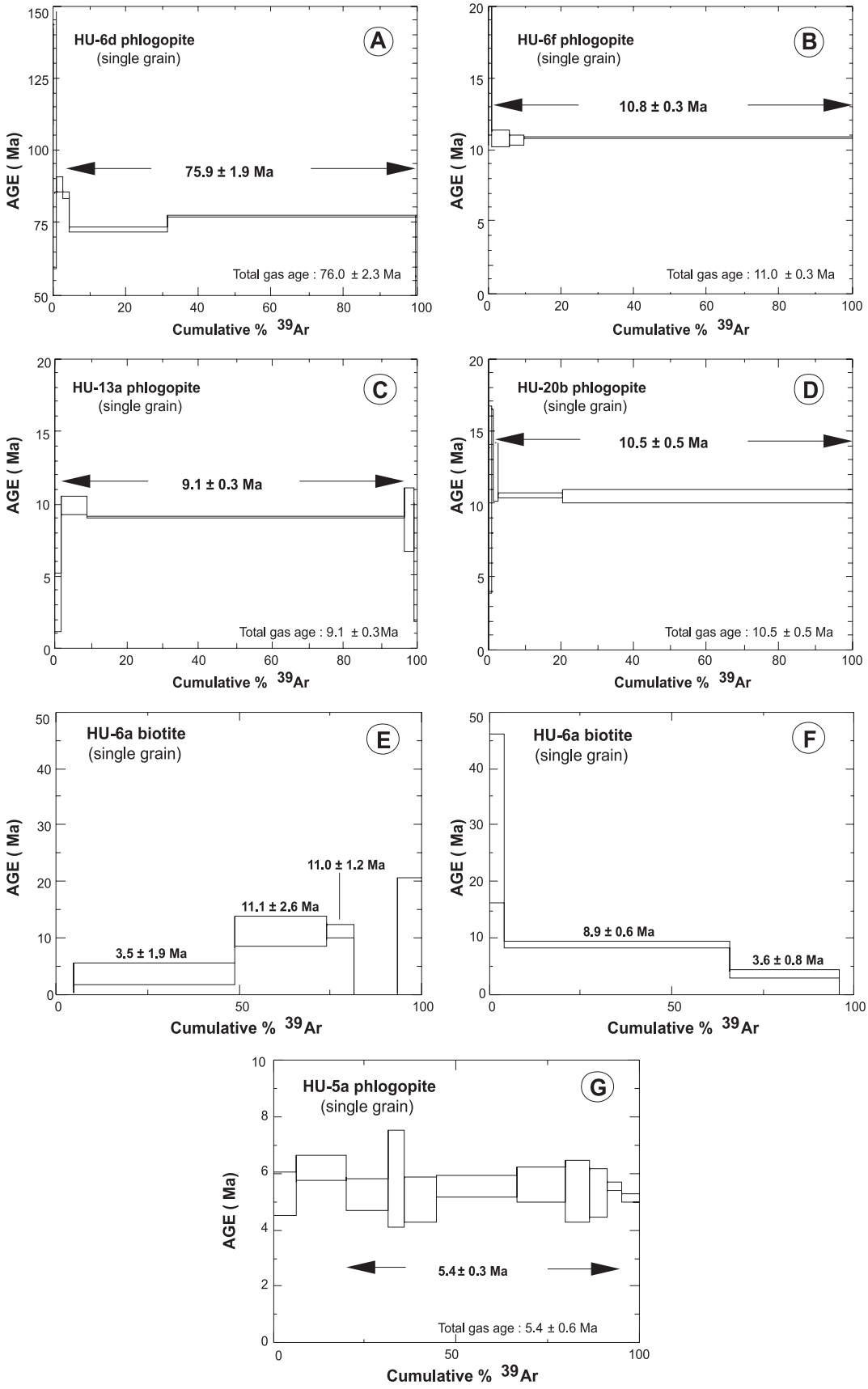

Fig. 10. Geological map of the Gosaikund Nappe and the Kathmandu basin, Nepal (modified from Rai 1998, 2001). (A) Location of the study area. (B) Detail of the area with the Ruyil and Chumar ruby occurrences and the Paigutan Pb–Zn deposit. MBT, Main Basal Thrust; MCT, Main Central Thrust; MT, Mantle Thrust.

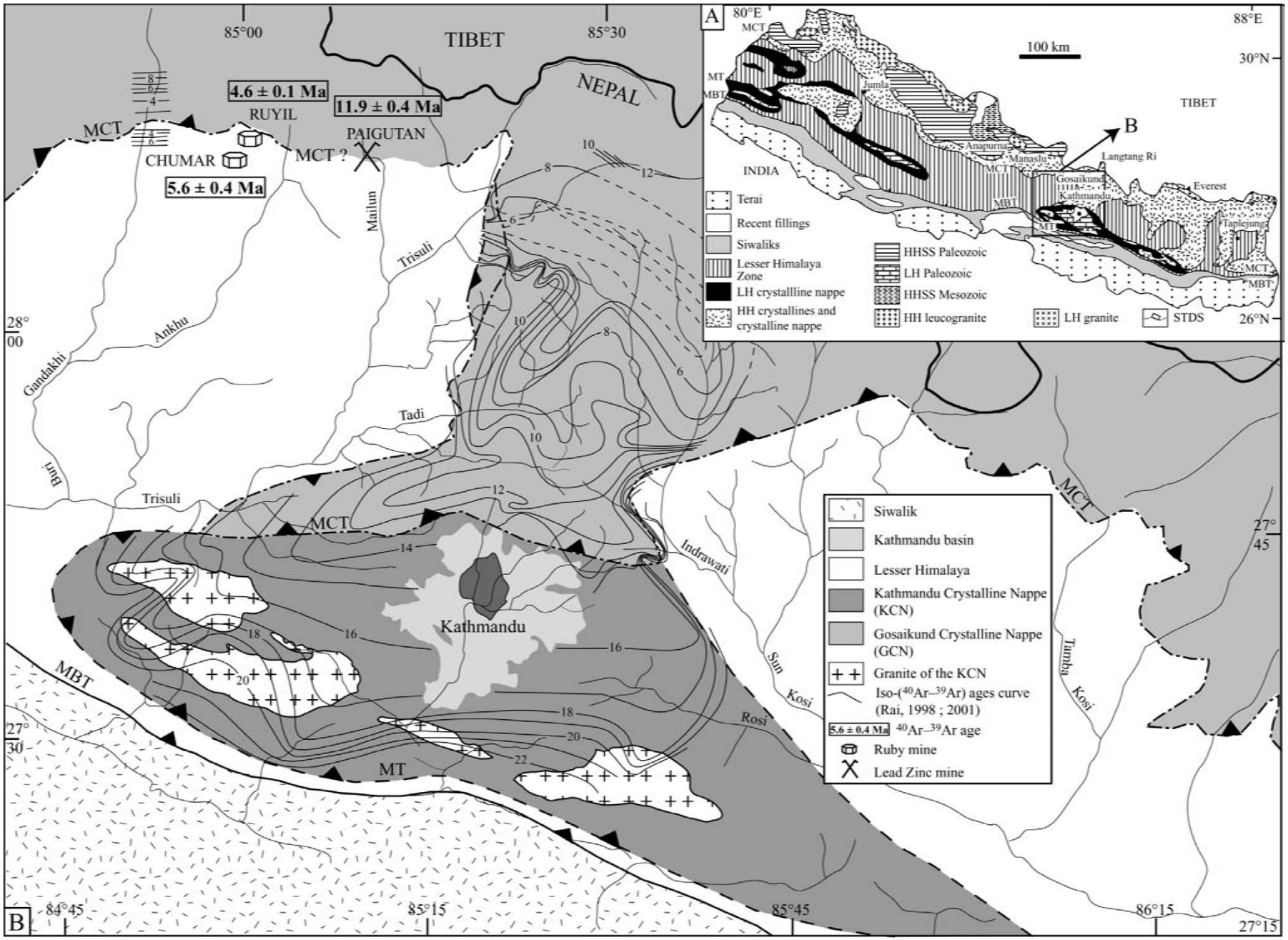

Fig. 11. ^{40}Ar–^{39}Ar age spectra of phlogopites from ruby-bearing marbles from Ruyil and Chumar, Nepal. Ar–Ar plateau ages are reported. Arrows indicate the extent of the Ar–Ar plateau.

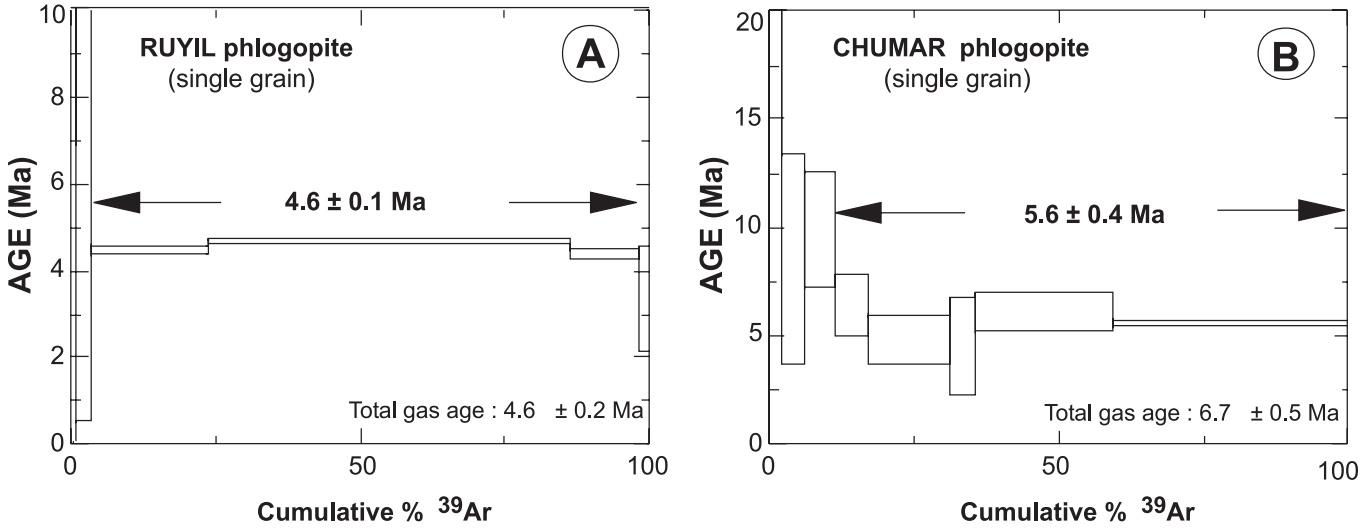

Fig. 12. Structural map of Myanmar and surrounding regions (modified from Bertrand et al. 2001) showing ^{40}Ar–^{39}Ar ages of the metamorphic rocks, including the ruby-bearing marbles from the Mogok metamorphic belt.

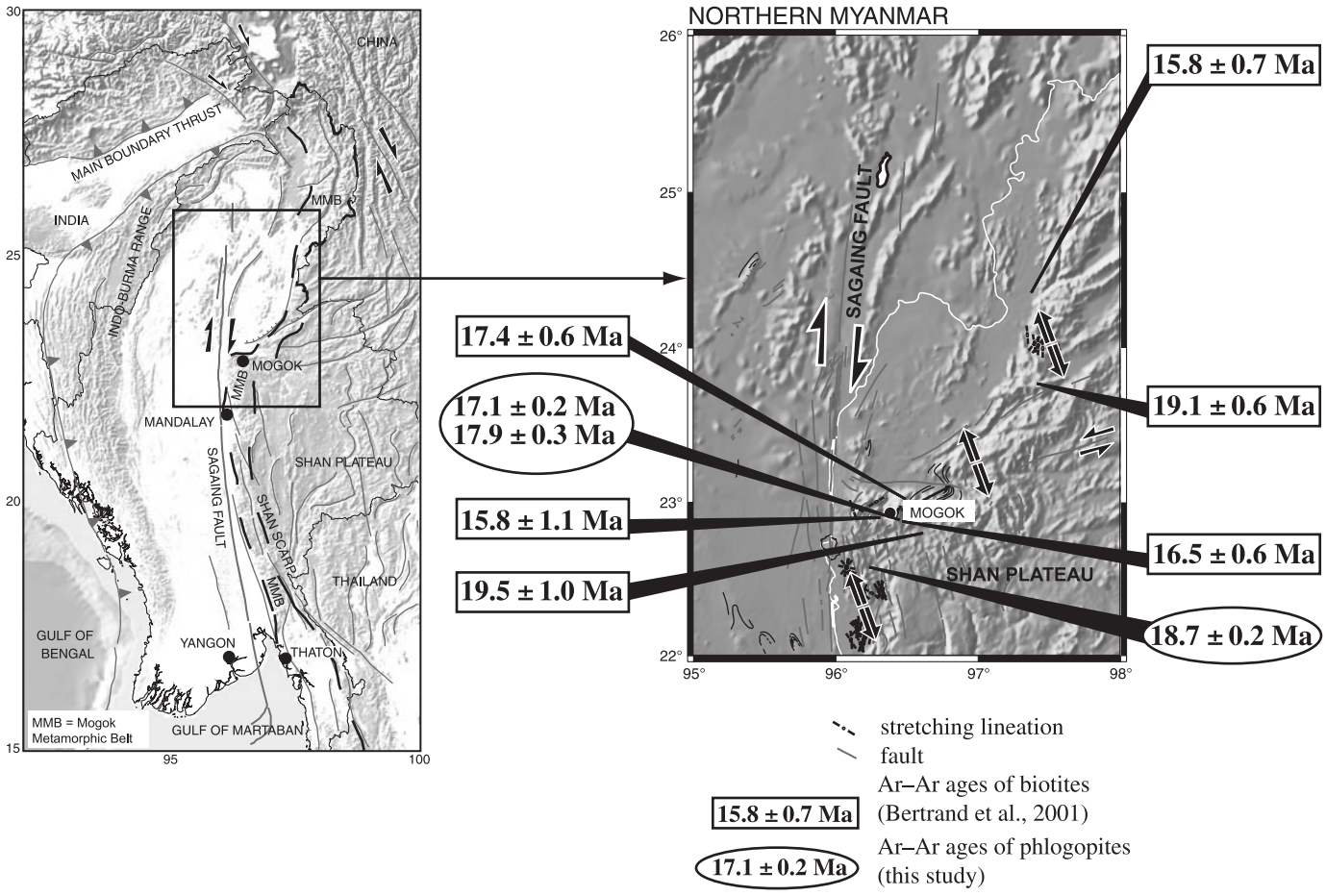

Fig. 13. (A, C, D) Cathodoluminescence-images and (B) back-scattered electron image from typical zircon crystals from the Quy Chau placers, Vietnam. Analytical spots and U–Pb ages are reported. ^{238}U–^{206}Pb, bold; ^{235}U–^{207}Pb, not bold.

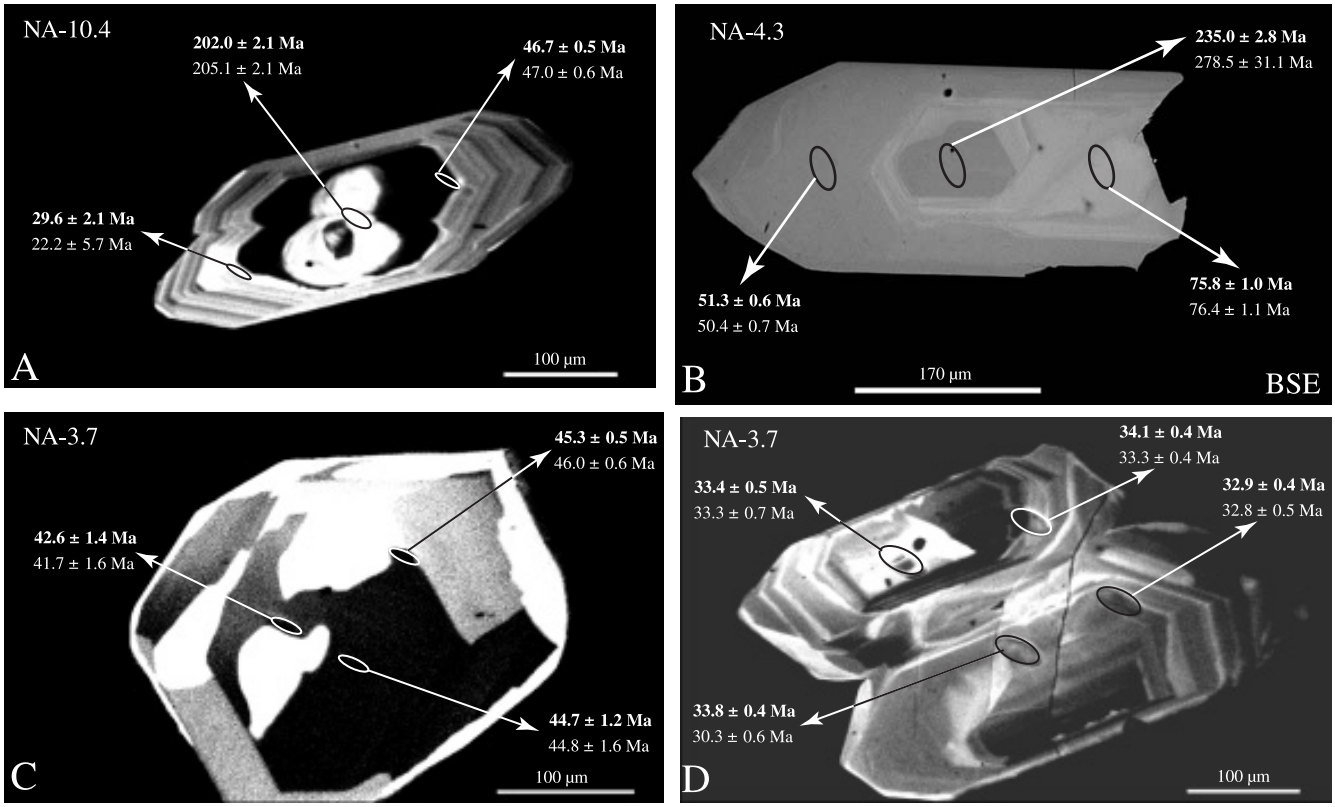

Fig. 14. Histogram of frequency distribution of the ^{238}U–^{206}Pb ages obtained on the zircon crystals from Quy Chau ruby-placers, Vietnam. The age obtained on a zircon included in a ruby from those placers is reported.

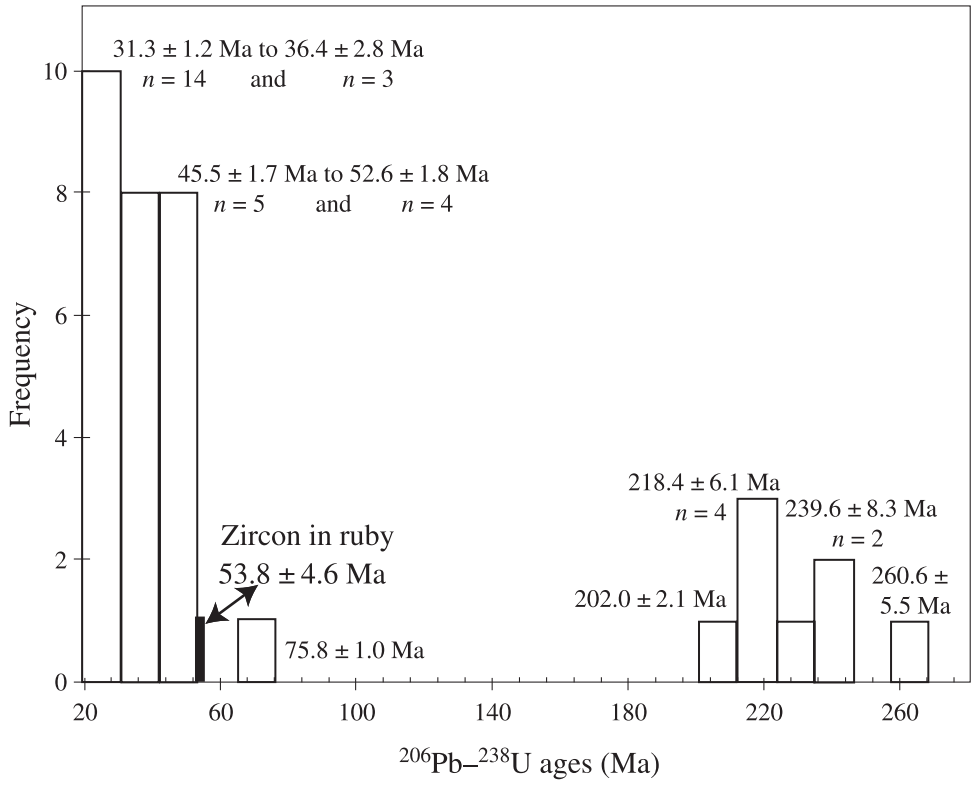

ages, which are related to the extrusion of the central deep-crustal pop-up corner of the Nanga Parbat massif. The Mogok deposits also formed in Early Miocene, during the extensional tectonics that are related to the migration of the eastern Himalayan syntaxis. Rubies from Nepal formed at the end of the Miocene during late activity on the MCT.

(3) Cenozoic ages for ruby formation in marbles from Asia imply the existence of a high-quality ruby belt running from Afghanistan to Vietnam. This metallogenetic ruby belt has a unique genetic history, resulting from the high-temperature metamorphism that developed during the Eocene continental collision between India and Eurasia. The specific time of formation of each deposit depended on its location within the Himalayan belt.

Acknowledgments

This study was supported by the Institut pour la Recherche et le Développement, Centre National de la Recherche Scientifique (Centre de Recherches Pétrographiques et Géochimiques), the Programme International de Coopération Scientifique (CNRS – Institut National des Sciences de l'Univers, and Center for Natural Sciences and Technology) program, the French Foreign Office and the French Embassy in Pakistan in cooperation with the Geological Survey of Pakistan (Project DSUR-PAK-4C5-013). We thank the Vietnamese Basic Research Program on the Geodynamics of the Red River fault zone for its assistance. The authors are grateful to Dr A.B. Kausar (Geological Survey of Pakistan), Dr. Phan Trong Thrinh and Hoàng Quang Vinh (National Center for Natural Sciences and Technology, Hanoi, Vietnam), and Dr. Pham Van Long (Vietnam National Gem and Gold Corporation) for their assistance in the field, and to Dr. B. Goffé (Ecole Normale Supérieure, Paris, France) for access to his samples from Mogok in Myanmar. We thank S. Barda, Dr. F. Diot, and A. Kohler (University Henri Poincaré, Nancy) for SEM images and microprobe analyses; Dr. E. Deloule, Dr. M. Champenois, and D. Mangin (CRPG) for their help in using the ion-probe. We are grateful to Dr. L. Reisberg (CRPG-CNRS) for improving the English. We also thank Dr. L. Groat (The University of British Columbia, Vancouver, B.C.) and Dr. A. Camacho (Queen's University, Kingston, Ontario) for correction and improvement of the manuscript, and Dr. W.J. Davis (Geological Survey of Canada, Ottawa, Ontario) for handling the manuscript.

References

Alexander, E.C., Mickelson, G.M., and Lamphere M.A. 1978. MMHB-1: a new $^{40}Ar/^{39}Ar$ dating standard. US Geological Survey, Open File Report 6-8.

Barley, M.E., Pickard, A.L., Khin Zaw, Pak, P., and Doyle, M.G. 2003. Jurassic to Miocene magmatism and metamorphism in the Mogok metamorphic belt and the India-Eurasia collision in Myanmar. Tectonics, **22**: 1019–1029.

Bender, F. 1983. Geology of Burma. Gebrüder Brontraeger Verlagsbuchhandlung Ed., Berlin, Germany.

Berman, R.G. 1991. Thermobarometry using equilibrium calculations: a new technique with petrologic applications. Canadian Mineralogist, **29**: 833–855.

Bertrand, G., and Rangin, C. 2003. Tectonics of the western margin of the Shan plateau (central Myanmar): implication for the India-Indochina oblique convergence since the Oligocene. Journal of Asian Earth Sciences, **21**: 1139–1157.

Bertrand, G., Rangin, C., Maluski, H., Han, T.A., Mint, T., Mint, H. et al. 1999. Cenozoic metamorphism along the Shan scarp (Myanmar): evidences for ductile shear along the Sagaing fault or the northward migration of the eastern Himalayan syntaxis? Geophysical Research Letters, **26**: 915–918.

Bertrand, G., Rangin, C., Maluski, H., and Bellon, H. 2001. Diachronous cooling along the Mogok Metamorphic Belt (Shan scarp, Myanmar): the trace of the northward migration of the Indian syntaxis. Journal of Asian Earth Sciences, **19**: 649–659.

Cherniak, D.J., and Watson, E.B. 2001. Pb diffusion in zircon, Chemical Geology, **172**: 5–24.

Copeland, P., Le Fort, P., Upreti, B., and Rai, S.M. 1997. Flexure of the Main Central Thrust in the Kathmandu area due to ramping of the Main Boundary Thrust. *In* 7th Annual Goldschmidt Conference, Tucson, Arizona, 2–6 June 1997. Abstract volume, p. 55.

Crawford, M.B., and Searle, M.P. 1993. Collision-related granitoid magmatism and crustal structure of the Hunza Karakoram, North Pakistan. *In* Himalayan tectonics. *Edited by* P.J. Treloar and M.P. Searle. Geological Society (of London), Special Publication 74, pp. 53–68.

Debon, F., Afzali, H., Le Fort, P., and Sonet, J. 1986. Plutonic belts in Afghanistan: typology, age and geodynamic setting. Mémoires des Sciences de la Terre, Nancy, 47, pp. 129–153.

Debon, F., Afzali, H., Le Fort, P., Sonet, J., and Zimmermann, J.L. 1987. Plutonic rocks and associations in Afghanistan. Typology, age and geodynamic setting. Mémoires des Sciences de la Terre, Nancy, 49, pp. 1–132.

Deloule, E., Alexandrov, P., Cheilletz, A., Laumonier, B., and Barbey, P. 2002. In-situ U–Pb zircon ages for Early Ordovician magmatism in the Eastern Pyrenees, France: the Canigou orthogneisses. International Journal of Earth Science (Geologisches Rundschau), **91**: 398–405.

Dilles, J.H., Snee, L.W., and Laurs, B.M. 1994. Geology, Ar–Ar age and stable isotope geochemistry of suture-related emerald mineralization, Swat, Pakistan Himalayas. Geological Society of America, Abstracts with Programs, **26**: 311.

Fraser, J.E., Searle, M.P., Parrish, R.R., and Noble, S.R. 2001. Chronology of deformation, metamorphism and magmatism in the Southern Karakoram Mountains. Geological Society of America Bulletin, **113**: 1443–1455.

Garnier, V. 2003. Les gisements de rubis associés aux marbres de l'Asie Centrale et du Sud-est: genèse et caractérisation isotopique. Ph.D thesis, INPL, Nancy, France.

Garnier, V., Giuliani, G., Maluski, H., Ohnenstetter, D., Phan Trong, T., Hoàng Quang, V. et al. 2002. Ar–Ar ages in phlogopites from marble-hosted ruby deposits in northern Vietnam: evidence for Cenozoic ruby formation. Chemical Geology, **188**: 33–49.

Garnier, V., Giuliani, G., Ohnenstetter, D., Kausar, A., Hoàng Quang, V., Phan Trong, T. et al. 2004. Les gisements de rubis du Pakistan et du Viêt-nam. Association Française de Gemmologie (AFG), **150**: 1–7.

Garnier, V., Ohnenstetter, D., Giuliani, G., Maluski, H., Deloule, E., Phan Trong, T. et al. 2005. Age and significance of ruby-bearing marbles from the Red River shear zone, Northern Vietnam. Canadian Mineralogist, **43**: 1483–1497.

Giletti, B.J. 1974. Studies in diffusion, I, Argon in phlogopite mica. *In* Geochemical transport and kinetics. *Edited by* A.W. Hofmann, B.J. Giletti, H.S. Yoder, Jr., and R.A. Yund. Carnegie Institute, Washington, D.C., pp. 107–115.

Gilley, L.D., Harrison, T.M., Leloup, P.H., Ryerson, F.J., Lovera, O.M., and Wang, J.H. 2003. Direct dating of left-lateral deformation along the Red River shear zone, China and Vietnam. Journal of Geophysical Research, **108**, part 2, section 2, p. ECVA4.

Giuliani, G., Dubessy, J., Banks, D., Hoàng Quang, V., Lhomme, T., Pironon, J. et al. 2003*a*. CO_2–H_2S–COS–S_8–AlO(OH)-bearing fluid inclusions in ruby from marble-hosted deposits in Luc Yen area, North Vietnam. Chemical Geology, **194**: 167–185.

Giuliani, G., Hoàng Quang, V., Lhomme, T., Dubessy, J., Banks, D., Fallick, A.E. et al. 2003*b*. CO_2–H_2S–COS–S_8–AlO(OH)-bearing fluid inclusions in ruby from marble-hosted ruby deposits in Luc Yen and Quy Chau, North Vietnam. Geological Association of Canada – Mineralogical Association of Canada Joint Annual Meeting, Vancouver, B.C., 25–28 May 2003, Abstract volume, p. 317.

Giuliani, G., Fallick, A.E., Garnier, V., France-Lanord, Ch., Ohnenstetter, D., and Schwarz, D. 2005. Oxygen isotopes as a tracer to the origin of rubies and sapphires. Geology, **33**: 249–252.

Harrison, T.M., Leloup, P.H., Ryerson, F.J., Tapponnier, P., Lacassin, R., and Chen, W. 1996. Diachronous initiation of transtension along the Ailao Shan-Red River shear zone, Yunnan and Vietnam. *In* The tectonic evolution of Asia. *Edited by* A. Yin and T.M. Harrison. Cambridge University Press, New York, N.Y., pp. 208–226.

Hauzenberger, C.A., Häger, T., Baumgartner, L.P., and Hofmeister, W. 2001. High-grade metamorphism and stable-isotope geochemistry of N-Vietnamese gem bearing rocks. International workshop on material characterisation by solid-state spectroscopy: gems and minerals of Vietnam, Hanoi, Vietnam, 4–10 April 2001. Astracts, pp. 124–138.

Hess, J.C., and Lippolt, H.J. 1994. Compilation of K-Ar measurements on HD-B1 standard biotite – 1994. Status report. *In* Phanerozoic time scale. *Edited by* G.S. Odin. Bulletin de Liaison et d'Information, International Union of Geological Sciences (IUGS) Subcommittee Geochronology, Vol. 12, Paris, France, pp. 19–23.

Hildebrand, P.R., Noble, S.R., Searle, M.P., Waters, D.J., and Parrish, R.R. 2001. Old origin for an active mountain range: Geology and geochronology of the eastern Hindu Kush, Pakistan. GSA Bulletin, **113**: 625–639.

Hughes, R.W. 1997. Ruby and sapphire. RWH Publishing, Boulder, Colo.

Jaffey, A.H., Flynn, K.F., Gledenin, L.F., Bentley, W.C., and Essling, A.M. 1971. Precision measurements of half-lives and specific activities of ^{235}U and ^{238}U. Physical Review, **C4**: 1889–1906.

Jolivet, L., Maluski, H., Beyssac, O., Goffé, B., Lepvrier, Cl., Phan Truong, T. et al. 1999. Oligocene–Miocene Bu Khang extensional gneiss dome in Vietnam: geodynamic implications. Geology, **27**: 67–70.

Jolivet, L., Beyssac, O., Goffé, B., Avigad, D., Lepvrier, C., Maluski, H. et al. 2001. Oligo-Miocene midcrustal subhorizontal shear zone in Indochina. Tectonics, **20**: 46–57.

Khan, F., Latif, M., Fayaz, A., and Khan, S.U.Z. 1987. Geology and minerals investigations of Hunza-Nagir area, Northern Areas, Pakistan. Geological Survey of Pakistan, Quetta, Pakistan, Report 291.

Le Fort, P., Debon, F., and Sonet, J. 1983. Petrography, geochemistry and geochronology of some samples from the Karakorum batholith (N. Pakistan). *In* Granites of the Himalayas, Karakoram and Hindu Kush. *Edited by* F.A. Shams. Punjab University, Lahore, India, pp. 377–387.

Leloup, Ph.H., Harrison, T.M., Ryerson, F.J., Wenji, C., Qi, L., Tapponnier, P. et al. 1993. Structural, petrological and thermal evolution of a tertiary ductile strike-slip shear zone, Diancang Shan, Yunnan. Journal of Geophysical Research, **98**(B4): 6715–6743.

Leloup, Ph.H., Lacassin, R., Tapponnier, P., Schärer, U., Dalai, Z., Xiaohan, L. et al. 1995. The Ailao Shan-Red River shear zone (Yunnan, China), tertiary transform boundary of Indochina. Tectonophysics, **251**: 3–8.

Leloup, Ph.H., Arnaud, N., Lacassin, R., Kienast, J.R., Harrison, T.M., Phan Trong, T. et al. 2001. New constraints on the structure, thermochronology and timing of the Ailao Shan-Red River shear zone, SE Asia. Journal of Geophysical Research, **106**(B4): 6683–6732.

Lepvrier, C., Maluski, H., Nguyen Van, V., Roques, D., Axente, V., and Rangin, C. 1997, Indosinian NW-trending shear zones within the Truong Son belt (Vietnam): ^{40}Ar–^{39}Ar Triassic ages and Cretaceous to Cenozoic overprints. Tectonophysics, **283**: 105–127.

Maluski, H., Lepvrier, C., Ta Trung, T., and Duc, T. 1999. Effect of up-doming process in the Song Chay Massif (Vietnam) on Ar–Ar ages. European Union Geosciences (EUG) 10, Strasbourg, France, 6–12 April 1999. Terra Abstracts, p. 57.

McDougall, I., and Harrison, T.M. 1988. Geochronology and thermochronology by the ^{40}Ar–^{39}Ar method. Clarendon Press, Oxford, UK.

Okrusch, M., Bunch, T.E., and Bank, H. 1976. Paragenesis and petrogenesis of a corundum-bearing marble at Hunza (Kashmir). Mineralium Deposita, **11**: 278–297.

Pêcher, A., Giuliani, G., Garnier, V., Maluski, H., Kausar, A., Malik, R.H. et al. 2002. Geology and geochemistry of the Nangimali ruby deposit area, Nanga-Parbat Himalaya (Azra Kashmir, Pakistan). Journal of Asian Earth Science, **21**: 265–282.

Rai, S.M. 1998. Les nappes de Katmandou et du Gosaikund, Himalaya du Népal Central (Étude cartographique, structurale, métamorphique, géochimique et radiochronologique). Ph.D. thesis, Université J. Fourier, Grenoble, France.

Rai, S.M. 2001. Geology, geochemistry, and radiochronology of the Kathmandu and Gosaikund Crystalline nappes, Central Nepal Himalaya. Journal of Nepal Geological Society, **25**: 135–155.

Rossovskiy, L.N. 1980. Gemstone deposits of Afghanistan. Geology of Ore Deposits, **22**(3): 74–88. (In Russian.)

Rossovskiy, L.N., Konovalenko, S.I., and Ananjev, S.A. 1982. Conditions of ruby formation in marbles. Geology of Ore Deposits, **24**: 57–66. (In Russian.)

Sabot, B., Cheilletz, A., De Donato, P., Archibald, D., and Barrès, O. 2002. Les gisements d'émeraude d'Afghanistan et du Pakistan : marqueurs de l'évolution de la chaîne himalayenne. Réunion Sciences de la Terre (RST) 2002, Nantes, France, 9–12 April 2002, Abstract volume, p. 207.

Schärer, U., Tapponnier, P., Lacassin, R., Leloup, P.H., Zhong, D., and Ji, S. 1990*a*. Intraplate tectonics in Asia: a precise age for large-scale movements along the Ailao Shan – Red River shear zone, China. Earth and Planetary Science Letters, **97**: 65–77.

Schärer, U., Copeland, P., Harrison, T.M., and Searle, M.P. 1990*b*. Age, cooling history, and origin of post-collisional leucogranites in the Karakorum batholith; a multi-system isotope study. Journal of Geology, **98**: 65–77.

Schärer, U., Lian-Sheng, Z., and Tapponnier, P. 1994. Duration of strike-slip movements in large shear zones: the Red River belt, China. Earth and Planetary Science Letters, **126**: 379–397.

Schneider, D.A., Edwards, M.A., Kidd, W.S.F., Zeitler, P.K., and Coath, C.D. 1999. Earth and Planetary Science Letters, **167**: 121–129.

Smith, C.P., Gübelin, E.J., Bassett, A.M., and Manandhar, M.N. 1997. Rubies and fancy-color sapphires from Nepal. Gems & Gemology, **33**: 24–41.

Stacey, J.S., and Kramers, J.D. 1975. Approximation of terrestrial lead isotope evolution by a two stage model. Earth and Planetary Science Letters, **26**: 207–221.

Steiger, R., and Jäger, E. 1977. Subcommission on geochronology: convention on the use of decay constants in geo-and cosmochronology. Earth Planetary Science Letters, **36**: 359–362.

Tapponnier, P., Lacassin, R., Leloup, Ph.H., Schärer, U., Dalai, Z., Haiwei, W., Schocheng, J., Lianshang, Z., and Iiayou, Z. 1990. The Ailao Shan/Red River metamorphic belt: Tertiary left-lateral shear between Indochina and South China. Nature, **343**: 431–437.

Terekhov, E.N., Kruglov, V.A., and Levitskii, V.I. 1999. Rare earth elements in corundum-bearing metasomatic and related rocks of the Eastern Pamirs. Geochemistry International, **37**: 202–212.

Wiedenbeck, M., Allé, P., Corfu, F., Griffin, W.L., Meier, M., Oberli, F., Von Quadt, A., Roddick, J.C., and Spiegel, W. 1995. Three natural zircon standards for U–Th–Pb, Lu–Hf, trace elements and REE analyses. Geostandard Newsletter, **19**: 1–23.

Zeitler, P.K., Chamberlain, C.P., and Smith, H.A. 1993. Synchronous anatexis, metamorphism, and rapid denudation at Nanga Parbat (Pakistan, Himalaya). Geology, **21**: 347–356.